First posted online on 27 November 2019 as 10.1242/jeb.201525
Access the most recent version at http://jeb.biologists.org/lookup/doi/10.1242/jeb.201525

Variation in limb loading magnitude and timing in tetrapods

Michael C. Granatosky[1], Eric J. McElroy[2], Pierre Lemelin[3], Stephen M. Reilly[4], John A. Nyakatura[5], Emanuel Andrada[6], Brandon M. Kilbourne[7], Vivian R. Allen[8], Michael T. Butcher[9], Richard W. Blob[10] and Callum F. Ross[11]

[1]Department of Anatomy, New York Institute of Technology, NY, USA
[2]Department of Biology, College of Charleston, Charleston, SC, USA
[3]Division of Anatomy, Department of Surgery, University of Alberta, Edmonton, AB, Canada
[4]Department of Biological Sciences, Ohio University, Athens, OH, USA
[5]Institut für Biologie, Humboldt-Universität zu Berlin, Berlin, Germany
[6] Institute of Zoology and Evolutionary Research, Friedrich-Schiller-University Jena, Germany
[7]Museum für Naturkunde, Leibniz Institut für Evolutions- und Biodiversitätsforschung, Invalidenstraße 43, 10115 Berlin, Germany
[8]Structure & Motion Lab, Department of Comparative Biomedical Sciences, The Royal Veterinary College, Hatfield, UK
[9]Department of Biological Sciences Youngstown State University, OH, USA
[10]Department of Biological Sciences, Clemson University, SC, USA
[11]Department of Organismal Biology and Anatomy, University of Chicago, Chicago, IL, USA

Corresponding Author:
Michael C. Granatosky
Department of Organismal Biology and Anatomy
The University of Chicago
1027 E 57th St, Chicago, IL 60637
Phone: (919) 599-7747
Email: mgranatosky@uchicago.edu

Keywords: Locomotion, sensorimotor, Golgi tendon organs, predictability, bradymetabolic, tachymetabolic

Abstract

Comparative analyses of locomotion in tetrapods reveal two patterns of stride cycle variability. Tachymetabolic tetrapods (birds and mammals) have lower inter-cycle variation in stride duration than bradymetabolic tetrapods (amphibians, lizards, turtles, and crocodilians). This pattern has been linked to the fact that birds and mammals share enlarged cerebella, relatively enlarged and heavily myelinated Ia afferents, and γ-motoneurons to their muscle spindles. Tachymetabolic tetrapod lineages also both possess an encapsulated Golgi tendon morphology, thought to provide more spatially precise information on muscle tension. The functional consequence of this derived Golgi tendon morphology has never been tested. We hypothesized that one advantage of precise information on muscle tension would be lower and more predictable limb bone stresses, achieved in tachymetabolic tetrapods by having less variable substrate reaction forces than bradymetabolic tetrapods. To test this hypothesis, we analyzed hindlimb substrate reaction forces during locomotion of 55 tetrapod species in a phylogenetic comparative framework. Variation in species-means of limb loading magnitude and timing confirm that, for most of the variables analyzed, variance in hindlimb loading and timing is significantly lower in species with encapsulated versus unencapsulated Golgi tendon organs. These findings suggest that maintaining predictable limb loading provides a selective advantage for birds and mammals by allowing for energy-savings during locomotion, lower limb bone safety factors, and quicker recovery from perturbations. The importance of variation in other biomechanical variables in explaining these patterns, such as posture, effective mechanical advantage, and center-of-mass mechanics, remains to be clarified.

Introduction

Comparative analyses of cyclical locomotion and chewing in tetrapods reveal two patterns of variation in cycle duration among tetrapods with different metabolic rates (Gintof et al., 2010; Ross et al., 2007; Ross et al., 2010; Ross et al., 2013). Tachymetabolic tetrapods, including birds and mammals, have relatively low levels of variation in stride duration between cycles—high rhythmicity—compared to bradymetabolic tetrapod lineages such as amphibians, lizards, turtles, and crocodilians (Ross et al., 2007; Ross et al., 2010; Ross et al., 2013). This higher rhythmicity in birds and mammals, which share a high metabolic rate (Nagy, 1987; Nagy, 2005; Nagy et al., 1999), is argued to be advantageous because it is more energetically efficient, postponing or minimizing fatigue in these highly active animals (O'Connor et al., 2012; Ross et al., 2013). Higher rhythmicity also allows for coordination and synchronization of cyclic movements, including tuning of locomotor and ventilation systems (Boggs, 2002; Carrier and Farmer, 2000; Nassar et al., 2001), coordination of jaw and tongue oscillations (Hiiemae and Palmer, 2003; Hiiemae et al., 1995; Palmer et al., 1997), and minimization of interlimb inference and obstacle avoidance during locomotion (Armstrong and Drew, 1985; Drew et al., 2002; Drew et al., 2004; English, 1989; Serrien et al., 2001).

The neuromuscular basis for high rhythmicity of the cyclic movements of birds and mammals is hypothesized to lie in the cerebellum, as well as in Ia afferents from and γ-motoneurons to muscle spindles (Ross et al., 2013). The cerebellum is an important regulator of predictive and responsive correction of external perturbations (Aoi et al., 2013; Butler and Hodos, 2005; Ross et al., 2013). Selective damage or degeneration of the cerebellum or its afferent and efferent neural pathways results in impaired interlimb coordination (Aoi et al., 2013; English, 1989; Fortier et al., 1987; Ichise et al., 2000; Morton and Bastian, 2006; Yanagihara et al., 1993). Birds and mammals have convergently evolved relatively enlarged lateral cerebella (Butler and Hodos, 2005), along with larger and more complex input and output nuclei (Appelberg et al., 1975; Johansson, 1988; ten Donkelaar, 1988; Wild and Williams, 2000).

Muscle spindle primary afferents–type Ia nerve fibers—convey information from muscle spindles to the central nervous system about the rate of change in the length of fibers within a muscle fascicle (Purves and Fitzpatrick, 2001). Afferent information about velocity changes in limb muscles is necessary for coupling limb movements to alternating bursts of motor activity from spinal central pattern generators (Verdaasdonk et al., 2006). Furthermore,

stronger afferent proprioceptive signals are associated with less variable cycle frequency (Ausborn et al., 2007). Deafferentation of spinal cord central pattern generators renders them incapable of compensating for variation in external forces and displacements associated with variably disrupted coordination (Allum et al., 1998; Grillner and Zangger, 1979; Grillner and Zangger, 1984; Wetzel et al., 1976). Bird and mammal type Ia afferents are myelinated and larger than those of other tetrapods, facilitating rapid conduction of spindle afferent information to the central nervous system (CNS) (Matthews, 1972; Prochazka et al., 2002; Romanovsky et al., 2007). Birds and mammals are also distinctive in having γ-motoneuron innervation of muscle spindle contractile elements, independent of the motor supply to the extrafusal fibers (Bilo et al., 1980; Hulliger, 1984; James and Meek, 1973; Maier, 1992; Ovalle, 1976; Proske, 1997). The γ-motoneurons allow spindle response properties to be tuned independently of extrafusal muscle activity in anticipation of movements and postural adjustments (Proske, 1997; Riemann and Lephart, 2002; Ross et al., 2013; Shneider et al., 2009).

In addition to their more enlarged cerebella, larger and myelinated type Ia afferents, and γ-motoneurons, the Golgi tendon organs (GTOs) of birds and mammals are also distinctive (Figure 1). The GTO is a specialized mechanoreceptor found in most skeletal muscles (Proske, 1979; Purves and Fitzpatrick, 2001). It lies in series between small groups of muscle fibers and their tendon or aponeurosis of origin or insertion (Huber and Dewitt, 1900; Proske, 1979). Typically, GTOs are distributed unevenly across muscle-tendon junction, most densely concentrated in the deep areas of the muscle (Horcholle-Bossavit et al., 1990; Mileusnic and Loeb, 2009). Often considered a protective organ, GTO's are known to be responsive over a wide range of normal physiological muscle forces (Crago et al., 1982; Houk and Henneman, 1967; Mileusnic and Loeb, 2009; Proske, 1979), so it is likely that GTOs have dual sensory roles in the protective Golgi tendon reflex at larger forces and in maintaining consistent limb loading conditions during normal behaviors (Alneas, 1967; Crago et al., 1982; Houk and Henneman, 1967; Mileusnic and Loeb, 2009). Golgi tendon organs are present in the tendons of fishes, amphibians, reptiles, birds, and mammals (Huber and Dewitt, 1900; Proske, 1979). The GTOs of most bradymetabolic tetrapods are free-endings located in tendons some distance from the muscle-tendon junction (Gregory and Proske, 1975; Huber and Dewitt, 1900; Proske, 1979), suggesting that they signal levels of tension across the whole muscle (Proske, 1979). In contrast, in birds and mammals encapsulated tendon organs are located directly at the muscle-tendon junction (Gregory et al., 2002; Haiden and Awad, 1981; Huber and Dewitt, 1900; Proske, 1979) where muscle fibers

insert into collagen bundles lying within the receptor capsule. This anatomical arrangement enables fine-scale signaling of tension in discrete portions of limb muscles (Mileusnic and Loeb, 2009), allowing more precise CNS control and predictability of forces generated by the muscles (Alneas, 1967; Crago et al., 1982; Houk and Henneman, 1967; Mileusnic and Loeb, 2009). Interestingly, the GTOs of turtles exhibit features resembling both bradymetabolic and tachymetabolic tetrapods, where some encapsulation of the GTOs is visible near the muscle-tendon junction, but non-encapsulated or free-endings are also present deeper in the tendon (Huber and Dewitt, 1900). Currently, we know little about the GTO morphology of crocodilians and monotremes.

Differences in rhythmicity between tachymetabolic and bradymetabolic tetrapods have been identified in limb step cycle durations (Granatosky et al., 2018a; Ross et al., 2013), but these data do not directly refer to variability in the locomotor forces that afferent information from spindles and GTOs is used to control. One important question is whether substrate reaction forces are also less variable in taxa with low variation in step cycle durations. Maintaining a predictable limb loading environment may have important consequences for overall costs of locomotion (O'Connor et al., 2012; Verdaasdonk et al., 2006), limb bone safety factors (Bertram and Biewener, 1988; Blob et al., 2014; Lowell, 1985), and the ability to recover from unexpected obstacles or perturbations to locomotion (Daley et al., 2006). These factors may be especially important for birds and mammals, which have greater daily travel distances (Daley et al., 2016; Jedrzejewski et al., 2001; Klaassen et al., 2008; Rowcliffe et al., 2012; Stark et al., 2005; Thompson, 1992; Thompson et al., 1999) and higher metabolic costs than bradymetabolic tetrapods (Nagy, 1987; Nagy, 2005; Nagy et al., 1999). In this study, we use hindlimb substrate reaction forces collected during locomotion of 55 tetrapod species to test the following hypothesis: *tetrapods with encapsulated Golgi tendon organs have less variable substrate reaction forces than species with unencapsulated Golgi tendon organs*. Corroboration of this hypothesis would support links between the degrees of rhythmicity in cycle duration and predictability in the forces acting on the hindlimbs during locomotion.

Materials and Methods

Kinetic data were collected from 55 tetrapod species (Figure 2). All data collection protocols were approved by the relevant IACUCs and followed previously published methods (Andrada et al., 2015; Bishop et al., 2018; Butcher and Blob, 2008; Granatosky, 2018;

Granatosky and Schmitt, 2019; Granatosky et al., 2016; Granatosky et al., 2018b; McElroy et al., 2014; Nyakatura et al., 2014; Nyakatura et al., 2019; Schmitt, 1999; Schmitt and Hanna, 2004; Sheffield and Blob, 2011; Sheffield et al., 2011), so are only summarized below. Limb loading data collected from common quails (*Coturnix coturnix*) by Andrada and colleagues (2014a) were downloaded from Dryad Digital Repository (Andrada et al., 2014b). Data from most other bird species (see Supplemental Table 1) were taken from Bishop et al. (2018).

Hindlimb forces were collected while animals moved on a flat runway or raised horizontal pole. All data for birds were collected during bipedal locomotion, while all other species used quadrupedal gaits. Substrate type was chosen based on the most commonly used substrate in the wild (see Supplemental Table 2). A small sub-section of the runway or pole was instrumented with either Kistler force plates (models 9317B or 9281B; Kistler Instrument Corp., Amherst, NY), an AMTI multi-axis force plate (MC3A-100, AMTI, Watertown, MA), or custom-made force platforms (K&N Scientific, Guilford, VT, USA and Bertec Corp., Columbus, OH, USA) (Andrada et al., 2014a; Andrada et al., 2015; Bishop et al., 2018; Butcher and Blob, 2008; Granatosky, 2018; Granatosky et al., 2016; Granatosky et al., 2018b; McElroy et al., 2014; Nyakatura et al., 2019; Schmitt, 1999; Schmitt and Hanna, 2004; Sheffield and Blob, 2011; Sheffield et al., 2011). Force plate output was sampled at 500 – 12,000 Hz, imported, summed and processed using BioWare™ v.5.1 software, and then filtered (low-pass Fourier, 60 Hz) and analyzed in MATLAB (Mathworks, Natick, MA). Only step cycles with single-limb contacts on the plate or those steps in which hindlimb forces could be clearly differentiated were analyzed.

During all new trials analyzed for this study, animals were video-recorded from a lateral view at 60 – 125 Hz. Only strides in which the animal was traveling in a straight path and not accelerating or decelerating (i.e., steady-state locomotion) were selected for analysis. Steady-state locomotion was determined by calculating the instantaneous velocity of a digitized point on the head between subsequent video frames throughout the entire stride, and then using regression analysis to determine whether velocity changed during the stride (Granatosky, 2015; Granatosky and Schmitt, 2019). Only strides in which no change in speed (i.e., slope not significantly different than zero) was detected were analyzed.

From these data, five variables were calculated for each single hindlimb substrate reaction force: (1) Braking peak (Bpk) force; (2) Propulsive peak (Ppk) force; (3) Medial peak (Mpk) force; (4) Lateral peak (Lpk) force; and (5) Vertical peak (Vpk) force. Additionally, the times at which Bpk, Ppk, braking to propulsive transition (B/P), Mpk, Lpk,

and Vpk, occurred during stance phase were also recorded. All force data were normalized for the direction of travel, differing body mass, and whether the limb that touched the instrumented portion of the runway was left or right. This resulted in comparable force curves that all displayed vertical force as a positive value on the vertical axis, braking force as a negative value on the fore-aft axis, propulsive force as a positive value on the fore-aft axis, medially oriented substrate reaction force as a negative value on the mediolateral axis, and laterally oriented substrate reaction force as a positive value on the mediolateral axis. In order to make comparisons between subjects of differing body masses, all force traces were converted into a proportion of the animal's body weight (% bw).

Inter-cycle variation in limb loading was assessed using the coefficient of variation (CV^*) of peak forces and of the timing of these peaks within each stance phase. Coefficients of variation were calculated within individuals (Supplemental Table 3) for each species using $CV^* = \left(1 + \frac{1}{4n}\right) CV$, where *n* is equal to the number of strides. The CV^* of stride cycle duration was also calculated for each individual. The inclusion of *n* in the calculation of CV^* provides an unbiased approximation of relative variance when sample size is low (Sokal and Rohlf, 2012). Due to the limited number of isolated hindlimb substrate reaction forces available for *Pleurodeles waltl* (i.e., one hindlimb substrate reaction force per individual) data for this species were combined for all statistical analyses. The CV^* of stride cycle duration for *Pleurodeles waltl* was calculated from data in Karakasiliotis et al. (2016) and for *Recurvirostra avosetta*, *Haematopus ostralegus*, and *Vanellus vanellus* from data in Kilbourne et al. (2016).

For all analyses, variables were $\log_{10}$-transformed to more closely approximate normality and reduce the potentially confounding effects of extreme values (Keene, 1995; Sokal and Rohlf, 2012). The species-mean $CV^*$of all limb loading variables and stride cycle durations were compared between species with unencapsulated versus encapsulated GTOs using a series of Mann–Whitney *U* tests. Despite an attempt to approximate normality in the dataset via $\log_{10}$-transformation, the Mann–Whitney *U* test remained the preferred conservative method of analyses due to small sample sizes (e.g., 55 species) (Sokal and Rohlf, 2012). Mann–Whitney U tests were conducted in MATLAB (v.2017b; MathWorks, Natick, MA, USA). Although information about GTO morphology is lacking for crocodilians, data collected from *Caiman crocodilus* were analyzed along other bradymetabolic tetrapods following Ross et al. (2013).

It is important to note that several variables are thought to affect variation in force magnitudes and timing (see Supplemental Table 2). Consequently, it may be the case that statistical differences observed via Mann–Whitney *U* testing described above do not effectively address the potentially influential effects of these confounding variables. As such, we conducted a series of linear mixed-effects models to assess the relationship between the variables of interest with species nested within GTO morphology as a random effect, and GTO morphology (i.e., encapsulated versus unencapsulated), substrate, number of hindlimb substrate reaction forces analyzed, body mass, and contact time as fixed effects. As it is well known that speed has a substantial effect on both force magnitude and the shape of force profiles (but see Supplemental Figures 1 and 2), it is important to consider speed and variation in speed as additional fixed effects. However, because of the large disparity of body sizes analyzed within this study, considering speed and variation in speed without considering potential scaling effects is untenable. As such, dimensionless speed (i.e., speed/√acceleration due to gravity x leg length) and variation in dimensionless speed were utilized instead and included in the model as additional fixed effects. Hindlimb length for each individual was determined either from direct measurements from the animals, calibrated space in video-recordings, the literature (Karakasiliotis et al., 2016), or based on a closely related taxon (hindlimb length for *Ambystoma mexicanum* was based off data from *A. tigrinum*). Preliminary model runs included the interaction between GTO morphology and mass, dimensionless speed, dimensionless speed CV^*, and contact time; however, these interactions were only rarely significant (3 out of 44). This indicates that the slope of relationships between limb loading/timing CV and mass, dimensionless speed, dimensionless speed CV^* and contact time does not differ between GTO morphologies. Thus, none of these interactions were included in the full models. As the goal of this study is to investigate the influence that GTO morphology has on limb loading magnitude and timing, we constrained comparison of our full model to a single null that did not include GTO morphology as a fixed effect nor did it include the GTO nesting (i.e., species was an un-nested random effect in the null model). The Burnham and Anderson (2001) approach for model comparison was used and Akaike's information criterion (AIC) generated for each model. Akaike's information criterion provides a measure of the goodness of fit of an estimated model and an operational way of trading off the complexity of an estimated model against how well the model fits the data. The best model has the lowest AIC and the significance of full models versus the null models were tested using likelihood ratio tests. Linear mixed-effects models were constructed and analyzed in R using "lme4" (Bates et al., 2014) following Winter (2013). Individual CV^*

for each of the variables of interest were used to construct linear mixed-effects models. Mass, dimensionless speed, dimensionless speed CV, contact time, and number of trials were centered and scaled prior to analysis.

Phylogenetic relatedness between sample taxa may influence these statistical analyses (Felsenstein, 1985; Garland et al., 1992), so we took the following steps to account for these effects in our comparisons. First, we generated a sample of 100 phylogenetic trees to account for phylogenetic uncertainty using the template of a recently published study on European tetrapods (Roquet et al., 2014). To do this, we first built the trunk of the phylogenetic tree to include the most recent common ancestor (*mrca*) of each of the following crown groups: Amphibia, Mammalia, Lepidosauria, Testudines, Crocodylia and Aves. Tree topology was fixed to widely accepted relationships among these major groups and the depth of each *mrca* node was fixed to the mean value reported at www.timetree.org (Hedges et al., 2006; Hedges et al., 2015; Kumar and Hedges, 2011; Kumar et al., 2017). Next, we grafted samples of trees for each crown group onto this trunk. To do this, we retrieved 1000 posterior samples of trees from www.vertlife.org/phylosubsets that were generated from phylogenetic analyses of squamates (Tonini et al., 2016), birds (Jetz et al., 2014) and amphibians (Jetz and Pyron, 2018). We used a posterior sample of 100 trees for mammals (Kuhn et al., 2011), which are based on a recent supertree analysis (Hedges et al., 2006; Hedges et al., 2015; Kumar and Hedges, 2011; Kumar et al., 2017). Our dataset had three turtle species, therefore we set the branching time between these taxa using values from www.timetree.org (Hedges et al., 2006; Hedges et al., 2015; Kumar and Hedges, 2011; Kumar et al., 2017). We then randomly chose one sample of each of these trees, then grafted them onto the appropriate node. We repeated this procedure 100 times to produce a posterior sample of 100 trees that accounted for uncertainty in branch lengths and topology. These trees were not ultrametric due to the decimal precision of the branch length estimates in the grafted trees; therefore, we forced them to be ultrametric by adding small amounts of branch lengths as needed (see http://blog.phytools.org/2017/03/forceultrametric-method-for-ultrametric.html for additional explanation). The final sample of 100 ultrametric, dated phylogenetic trees was used in all subsequent analyses. The maximum clade credibility tree from this sample had 100% nodal support for all nodes except for: 1) the node connecting *Varecia variegata*: *Lemur catta*, which had 60% support and 2) the node connecting *Meleagris gallopavo* and *Gallus gallus*, which had 52% support. The results of subsequent comparative analyses are presented as the mean ± standard deviation of the test statistic as computed from the sample of 100 trees. R-

packages used to construct the trees included "ape" (Paradis et al., 2004) and "phangorn" (Schliep, 2011).

We tested if species-mean $CV^*$of limb loading variables and stride cycle duration differed between tetrapods with encapsulated versus unencapsulated Golgi tendon morphology by fitting four different evolutionary models to our data given our sample of phylogenetic trees. The first two models were a single rate Brownian motion model (BM-1) and a single optimum Ornstein-Uhlenbeck model (OU-1) (Hansen, 1997). The BM-1 model assumed that the $CV^*$of all limb loading variables and stride cycle duration evolved under a single evolutionary rate. The OU-1 model assumed that only a single evolutionary trait optimum (i.e., one type of Golgi tendon morphology) was present with a parameter α pulling trait evolution towards that optimum. The other two models we fit were a two rate Brownian motion model (BM-M) and a two optimum Ornstein-Uhlenbeck model (OU-M). To fit the BM-M and OU-M models, we assumed that the ancestral condition for tetrapods was to have unencapsulated Golgi tendon organs and that the mammalian and avian lineages independently evolved encapsulated Golgi tendon organs, and then 'painted' the internal branches of the phylogeny accordingly (Figures 2-5). We fit these models over the sample of 100 trees and then computed the mean and standard deviation of parameter estimates across the 100 model fits. To determine which model (BM-1, BM-M, OU-1, or OU-M) was the 'best' fit to the data, we computed the small-sample size AIC for each model and computed Akaike weights from the AIC scores (Burnham and Anderson, 2001). We note that majority support for either the OU-M or BM-M model(s) would indicate that metabolic type was an important predictor of the evolution of $CV^*$of limb loading variables and/or stride cycle duration.

We ran these evolutionary models using two different inputs. First, we used the function phyl.resid in *phytools* (Revell, 2012) to fit a phylogenetic, multiple least squares regression with $\log_{10}$ transformed species mean values for $CV^*$of limb loading variables and stride cycle duration as the responses (separate regression for each response), and with $\log_{10}$ mass, dimensionless speed and dimensionless speed CV^* as predictors, all whilst accounting for phylogeny and assuming a Brownian motion model of trait covariance. This function returned a vector of species residuals, which can be interpreted as mass, dimensionless speed, and dimensionless speed CV^* 'corrected' values. These residuals were then used as input for the first set of evolutionary models listed above. For the second set of evolutionary models, we incorporated sampling error because it can have an important impact on analysis (Ives et

al., 2007). To do this, we fit models to the $\log_{10}$ transformed species mean values for $CV^{*}$of limb loading variables and stride cycle duration. We used squared standard errors as our estimate of sampling error. Standard errors were computed per species by first computing the mean CV^{*}per variable within each individual sampled and then computing the per species standard deviation and then dividing that standard deviation by the square root of the number of individuals sampled within that species. Some species had only one sampled individual, and thus their standard error could not be computed using this method. For these species, we assumed a standard error that was the arithmetic mean of all other species standard errors. Unfortunately, neither set of models is 'ideal'. The first set of models accounts for covariates that may influence force or cycle duration variables, but we are unaware of a method to account for species level 'error' in the residuals used as input for the first set of models. The second set of models can account for 'error' but does not adjust for covariates. In the context of these caveats, we fitted the evolutionary models using the mvMORPH package (Clavel et al., 2015).

We computed type I error rates and statistical power for the OU-M models using a simulation approach (Boettiger et al., 2012; Cooper et al., 2016; Schmitz and Higham, 2018). We did this by simulating 100 data sets under a BM-1 model of evolution and an additional 100 data sets under an OU-M model. Starting values for each model were derived from the fit of the first model from our analyses done over the sample of 100 trees, and done separately for mass/dimensionless speed/dimensionless speed CV corrected limb loading variables, and for raw variables that accounted for intraspecific sampling error. We then fitted the simulated datasets using BM-1 and OU-M and used the results of these fits to compute: a) the proportion of BM-1 datasets fit with OU-M models that had lower AIC than BM-1 datasets fit with BM-1 models (type 1 error rate) and b) proportion of OU-M datasets fit with OU-M models that had lower AIC than OU-M datasets fit with BM-1 models (statistical power). We also computed selection opportunity (η), the discriminably ratio (ϕ) and the signal to noise ratio. These three variables are dimensionless quantities that can provide insight into statistical power when using OU-M models (Cressler et al., 2015). We compared our computed values for η, ϕ and the signal to noise ratio to those from a previous simulation study to help better understand our statistical power, given our relatively low sample size (Cressler et al., 2015).

To test whether variation in single limb loading affects overall system rhythmicity, we conducted a series of regression analyses to assess the relationship between species-mean

$\log_{10} CV^*$ for each of the limb loading variables and CV^* of stride cycle duration. A series of phylogenetic least squares regression (PGLS) analyses was also conducted to account for the effect of phylogeny on these relationships using the R-package phylolm (Ho and Ané, 2014). Covariance in the PGLS was modeled using Pagel's λ and using a single-optimum Ornstein-Uhlenbeck model, so two PGLS models were fit for each limb loading variable. For the Pagel's λ model, λ can vary between 0 and 1, with 0 being a branch length transformation resulting in a star phylogeny and a λ of 1 resulting in the original phylogeny. Thus, a model fit using Pagel's λ estimates the phylogenetic signal in the regression and transforms branch lengths accordingly. We checked for normality and homoscedasticity of the residuals using diagnostic plots, and no issues were detected. Model fit for each variable was compared using Akaike weights. The *P*-values of the slope estimates for the best fitting models were corrected for multiple comparisons using the false discovery rate (Benjamini and Hochberg, 1995).

Results

We analyzed 1,930 hindlimb substrate reaction forces collected from 150 individuals. As found previously, CV^* of stride cycle duration is lower in animals with encapsulated Golgi tendon organ (GTO) morphology (Figure 3). On average, tachymetabolic tetrapods with encapsulated GTO morphology (i.e., mammals and birds) also experience lower variation in peak force magnitude and the timing at which those peak forces occur compared to bradymetabolic tetrapods with unencapsulated GTOs (i.e., amphibians, lizards, turtles, and crocodilians) (Tables 1-3, Figures 4 and 5, and Supplemental Table 3).

Results from Mann–Whitney *U* tests reveal significant differences (all $P \leq 0.044$) based on GTO morphology for CV^* of stride cycle duration and all limb loading variables, except Lpk CV^* and the timing of Lpk CV^*. Linear mixed-effects models did reveal the importance of considering other variables in addition to GTO morphology when exploring the causes of variability in limb loading and timing, such as speed, variation in speed, contact time, number of strides, substrate, and body mass (Supplemental Table 4). However, in all cases, except in regards to the timing of Lpk and timing of Vpk CV^*, the inclusion of information about GTO morphology in the linear mixed-effects models resulted in significantly lower AICs (Table 3). Lower AICs indicate that consideration of GTO

morphology results in more parsimonious explanations for variability in limb loading and timing than a model that does not include GTO morphology.

The OU-M models were the best fit for six out of 12 limb loading and cycle duration CV^* variables when they were corrected for size, speed, and speed CV^* (Table 4). OU-1 models were the best fit for the other six limb loading and cycle duration CV^* variables, and in all of these cases OU-M models were the second best fit (Table 4). In the second set of models, which accounted for intraspecific sampling error but did not correct for body mass, speed and speed CV^*, the OU-M models were the best fit for the timing of Bpk CV^* timing of Ppk CV^*, timing of Lpk CV^* and timing of B/P CV^*; while BM-M models were the best fit for timing of Vpk CV^* and Bpk CV^*. OU-1 and BM-1 models were the best fit for the other six variables (Supplemental Table 5). On average, the OU-M/BM-M models were favored in 50% of the cases, suggesting Golgi tendon organ morphology has evolved towards distinct optima and/or at distinct rates for some limb loading variables but not others. Simulations and computed values of η, ϕ and the signal-to-noise ratio all suggest moderate to high statistical power for most variables [Supplemental Table 6, but see Cressler et al. (2015) for a cautious note on interpreting these values], meaning that if an OU-M process generated the observed limb loading CV^* patterns, then we were likely to detect that process. However, simulations also found inflated type I error rates (mean = 0.17, range = 0.06-0.25) suggesting that we too often reject a BM-1 model when it might be the 'correct' evolutionary model. Phylogenetic half-life is reasonable for most of the OU-M and OU-1 models (i.e., in the range of the length of the tree, < 352 mya, Table 4), although some models that include standard error have a very large half-life, suggesting that traits will never reach their optima (Supplemental Table 5).

There is a significant relationship between CV^* of stride cycle duration and peak propulsive force CV^* (y = 0.29x + 0.81; P = 0.009), peak vertical force CV^* (y = 0.35x + 0.84; P = 0.005) and the timing of peak lateral force CV^* (y = -0.29x + 1.74; P = 0.016) (Supplemental Figure 3). PGLS models using Pagel's λ had the highest Akaike weight for all limb loading variables (Table 5). Pagel's λ was ~0.3-0.4, suggesting relatively weak phylogenetic signal in the relationships between CV^* of stride cycle duration and all limb loading variables. PGLS found no significant relationships between CV^* of stride cycle duration and limb loading variables after accounting for phylogenetic-relatedness of sample taxa (Table 5).

Discussion

In general, variance in peak force magnitude and the timing at which those peak forces occur was found to be lower in tachymetabolic tetrapods with encapsulated Golgi tendon organs (GTOs) (i.e., mammals and birds) compared to bradymetabolic tetrapods with unencapsulated GTOs. This is consistent with the hypothesis that birds and mammals have convergently evolved the ability to perceive precise information on muscle tension and as such can maintain a more predictable limb loading environment. That being stated, it is important to recognize several constraints on our experimental design that may limit the scope of its applicability. First, as with many studies that analyze force profiles, variation in locomotor speed across species, individuals, and trials can have substantial effects on the interpretation of results (e.g., Bishop et al., 2018; Demes et al., 1994; Granatosky and Schmitt, 2019; Granatosky et al., 2018b). Despite our use of dimensionless speed as a means to address this issue, it remains the case that one cannot discount speed and variation in speed entirely as an explanatory factor when exploring variability in limb loading and timing (Supplemental Table 4). However, in almost cases, the inclusion of information about GTO morphology in the linear mixed-effects models results in a more parsimonious explanation of the observed patterns in limb loading variation and timing across the species sampled. As such, we have observed no evidence suggesting that variation in locomotor speed across species, individuals, and trials in some way negates the major conclusions of this study. Though we addressed potentially confounding associations with dimensionless speed and dimensionless speed variation through statistical analyses, a more appropriate means of addressing this issue would have been more rigorous sampling at the initial experimental stages. Because this study used a combined dataset originating from multiple independent studies of freely moving animals, this was not possible. Future testing of the hypotheses presented here should take all possible precautions to assure similar speeds, gait types, and preferably Froude numbers between individuals, though this may be difficult to achieve across the full diversity of tetrapod species and body designs.

Another potential limitation was based on our goal to use data collected from animals moving on their preferred substrate (Supplemental Table 1). No data from arboreal bradymetabolic animals were available, raising the possibility that the observed differences are simply the result of locomotion on different substrates (i.e., arboreal vs. terrestrial). Our statistical analyses that account for differences in substrate use suggest no such conclusion, but data on the limb loading behavior of arboreal lizards currently being collected by Knight

and Lee (2019) and Munteanu et al. (2019) will help to address this issue. Related to this, postural differences among tetrapods have clear effects on the limb effective mechanical advantage, center-of-mass mechanics, limb kinematics, energetic savings from spring or pendular mechanisms, gait, and ecological use of locomotor behaviors [reviewed by Reilly et al. (2007)]. Any or all of these factors may explain differences among these taxa in the variation observed in substrate reaction forces, and their covariation makes disentangling their individual effects challenging. That being said, the sprawling locomotion of the common vampire bat (*Desmodus rotundus*) does not appear to influence inter-cycle loading variability compared to the other mammals sampled. Similarly, the "intermediate" postures used by *Caiman crocodilus* (Nyakatura et al., 2019) appear to do little to differentiate limb loading variation and timing of this taxa from other bradymetabolic tetrapods. Even though these are only two species, these data suggest that posture is less important in driving patterns in force variability than factors related to GTO morphology.

Finally, we acknowledge that our data underrepresent total tetrapod diversity and are skewed towards primates (14/55 species sampled) and tachymetabolic species broadly (39/55 species sampled). Data on forces and GTO anatomy are needed from a greater diversity of species, especially basal mammals, crocodilians and salamanders. Moreover, sampling more species may help to reduce the inflated type I error rates we found associated with the OU-M models (Cooper et al., 2016). Sampling GTO morphology and forces within a greater diversity of turtles would serve as a powerful test of the link between GTO morphology and force CV^* because it would control for metabolic type (i.e., all turtles are bradymetabolic) and it would limit the myriad of confounding variables inherent in sampling at a broad phylogenetic scope, such as all of Tetrapoda.

These concerns notwithstanding and as stated above, analyses of species-mean variation in limb loading magnitude and timing confirm that, for most of the variables analyzed, variance in hindlimb loading is significantly lower in animals with encapsulated versus unencapsulated GTOs. This difference is significant regardless of speed, variation in speed, contact time, number of individuals, number of strides, substrate, and body mass. This result has mixed support by the evolutionary analyses; the OU-M models that assume distinct evolutionary trait optima for animals with encapsulated versus unencapsulated GTOs are the best fit for ~ 50% of the limb loading variables. The large magnitudes of the differences in variance between animals with encapsulated versus unencapsulated GTOs in both peak hindlimb forces and the timing of those forces, as well as the persistence of these differences

across multiple lineages of birds and mammals, suggest that these clade-specific differences in limb loading provide insight into the functional significance of differences in rhythmicity. Specifically, maintaining a predictable limb loading environment may have important consequences for overall costs of locomotion (O'Connor et al., 2012; Verdaasdonk et al., 2006), bone safety factors (Bertram and Biewener, 1988; Blob et al., 2014; Lowell, 1985), and the ability to recover from unexpected falls (Daley et al., 2006). We address each of these in turn.

While the substrate reaction forces examined in this study do not provide a direct measure of force generation by the muscles, the external forces acting on the body during locomotion must be resisted by muscular activity (Beck, 2009; Gray, 1944; Gray, 1968). As such, variation in hindlimb substrate reaction forces provides insight into variation in muscle force production during locomotion. The energetic costs of moving the body constitute a high proportion of overall metabolic budget of an animal (Kram and Taylor, 1990; Pontzer, 2016; Reilly et al., 2007) and the predominant energy-consuming process in locomotion is muscle force production (Kram and Taylor, 1990; Pontzer, 2016). During locomotion on level substrates, muscle forces produced by limb muscles must support body weight and propel the animal forward. To optimize energy expenditure, animals should only apply the amount of force necessary to achieve support, balance, and propulsion (O'Connor et al., 2012; Taylor et al., 1980; Taylor et al., 1982) as increased variability in muscle force magnitudes wastes considerable amounts of energy (Agiovlasitis et al., 2015; Granatosky et al., 2018a; O'Connor et al., 2012; Verdaasdonk et al., 2006). Hence, minimizing variability in muscle force generation contributes to energetic efficiency during steady state locomotion.

Minimizing variation in substrate reaction forces also reduces the likelihood that oscillations of the center of mass and limbs will produce unstable dynamic states (Full et al., 2002; Jordan et al., 2007; O'Connor et al., 2012). In such states, avoiding falling and interlimb interference likely necessitates more muscle recruitment and more work by the limbs and their muscles. For birds and mammals, which have greater daily travel distances (Daley et al., 2016; Jedrzejewski et al., 2001; Klaassen et al., 2008; Marcus Rowcliffe et al., 2012; Stark et al., 2005; Thompson, 1992; Thompson et al., 1999) and higher metabolic costs than bradymetabolic tetrapods (Nagy, 1987,; Nagy, 2005; Nagy et al., 1999), minimizing unnecessary energetic expenditure by maintaining a predictable limb loading environment is likely to have had an important selective benefit.

During locomotion over land, limb bones are exposed to loads and, like most biological structures, they can withstand greater loads than they usually experience, as

estimated by their safety factor (Alexander, 1981; Alexander, 1988; Blob et al., 2014; Lowell, 1985). Among tetrapods, birds and eutherian mammals (opossums have safety factors consistent with bradymetabolic tetrapods; Butcher et al., 2011; Gosnell et al., 2011) have lower limb-bone safety factors than do other tetrapod lineages (Blob et al., 2014), possibly due to the greater predictability of the loads (Bertram and Biewener, 1988; Blob et al., 2014; Lowell, 1985). We hypothesize that improved predictability of dynamic loading facilitates the capacity of birds and mammals to operate successfully with lower limb bone safety factors, making it possible to reduce energetic costs as well (Alexander, 1997; Lowell, 1985).

The data presented here suggest that the limbs of birds and mammals experience reduced variability in external forces compared to other tetrapod lineages. We speculate that this is in part due to anticipatory modulation of reflexes through γ-motoneurons and enlarged cerebella, as well as to enhanced precision of their GTO system compared to other tetrapods (Gregory and Proske, 1975; Gregory et al., 2002; Haiden and Awad, 1981; Huber and Dewitt, 1900; Proske, 1979). At present, we know little about the control strategies that tetrapods use to maintain stability in the face of the unexpected obstacles they experience in their natural environment. Daley and colleagues (2006) addressed this question by perturbing the running of guinea fowl with an unexpected drop in substrate height. To avoid instability upon encountering a sudden drop the bird must dissipate energy, convert it to another form, or perform both in combination (Biewener and Daley, 2007; Daley et al., 2006). Interestingly, guinea fowl adopt a range of these strategies across a continuum that relates to magnitude and direction of the substrate reaction force. When animals experience an unexpected perturbation limb muscles must activate with the appropriate timing and intensity to resist substrate reaction forces and provide the appropriate leg stiffness (Daley et al., 2006). The activation level of the limb muscles depends on a combination of feed-forward, rhythmic motor control and proprioceptive feedback, including muscle stretch (spindle organs) and GTOs (Grillner, 1975; Pearson et al., 1998). The derived GTO morphology of birds and mammals and the increased predictability of rhythmic movements may allow birds and mammals to return to a state of dynamic stability after an unexpected fall quicker than animals with unencapsulated GTOs. Future work in this area is required to test this hypothesis.

While variation in limb loading does appear to be largely driven by differences in GTO morphology, the magnitude of this variation is largely variable dependent. Namely, propulsive and braking forces show the greatest disparity between species with encapsulated versus unencapsulated GTOs. This is followed by vertical forces, and much smaller

differences are observed in mediolateral forces, which tend to be highly variable across strides for all species. Arguably, there are functional reasons and consequences associated with these findings. As articulated by Bishop et al. (2018), mediolateral forces are probably only (or at least predominantly) exerted for stabilization purposes. That is, they reflect small-scale, step-to-step adjustments made by the animal in order to maintain dynamic stability. Therefore, rather than being an important motor goal to achieve straight-line locomotion, mediolateral forces may be viewed as a constraint: simply apply whatever mediolateral force is necessary at each instant in time to maintain dynamic stability. Furthermore, because mediolateral forces tend to be relatively small compared to vertical and fore-aft force components, even in sprawling taxa, small fluctuations about the mean result in substantially greater variance (Sokal and Rohlf, 2012). Vertical forces are usually the largest that an animal exerts and primarily serve to support the body against gravity (Gray, 1944). As such, maintaining appropriate vertical forces is essential to preventing an animal from collapsing. As a result, there is likely less room for variance in this loading parameter compared to the other force components. Both in terms of timing and magnitude, variation in propulsive and braking forces is greatest between sample taxa. These fore-aft forces functionally serve to keep the animal moving forward and inhibit out-of-control momentum of the center of mass (Granatosky et al., 2018b; Gray, 1944). Thus, propulsive and braking forces likely most influence overall system rhythmicity, which as discussed above, has clear selective advantages for birds and mammals. It is also the case the fore-aft forces most strongly correlate with overall external morphology of bony structures (Fabre et al., 2016). This relationship may explain the overlapping patterns in bone safety factors observed by Blob et al. (2014) and the findings of this study.

Conclusions

This study demonstrates that, in addition to having less variable cycle durations, tachymetabolic tetrapods (i.e., birds and mammals) also exhibit lower variation in limb loading magnitude and timing during locomotion compared to bradymetabolic tetrapods (i.e., amphibians and reptiles). The ability of birds and mammals to monitor and correct force variability could be linked to neural specializations such as encapsulated GTOs positioned near the muscle-tendon junction, along with the presence of γ–motoneurons and enlarged afferents and cerebella. We hypothesize that a predictable limb loading environment is advantageous for birds and mammals by allowing for energy-savings during locomotion, lower safety factors in limb bones, and quicker recovery from perturbations.

Acknowledgements

We thank the all those that helped with animal care and use. Without their help, we would not be able to complete this study. We thank Daniel Schmitt, JD Laurence-Chasen, Mark Westneat and two anonymous reviewers for their comments that improved the overall quality of this work.

Competing interests

The authors report no competing interests or conflict of interest.

Funding

This study was funded in part by the Leakey Foundation, Force and Motion Foundation, the National Science Foundation's Graduate Research Fellowship Program, and BCS 9706676, 0109130, 0240865, 0504685, 0725126, 0725147, 0962682.

Author contributions

MCG and CFR designed the study. MCG collected data and provided locomotor data from mammals. EJM and MCG conducted all statistical analyses. EJM and SMR provided data on reptile locomotion. JAN, EA, and VRA provided data from amphibians, crocodiles, and reptiles. JAN, EA and BMK provided data from birds. PL provided data for kinkajous and coatis. MTB and RWB provided data on turtles, tegus, and amphibians. MCG, EJM, PL, MTB, RWB, SMR and CFR wrote and edited the initial submission. MCG, EJM, PL, MTB, RWB, SMR, JAN, EA, BMK, VRA and CFR edited the revision.

Data accessibility

All data used in this study are provided in Supplemental Table 3. Additionally, data, phylogeny and R-scripts used for analyses are available via Figshare: https://figshare.com/s/e3095a4b07376797e92a.

Literature cited

Agiovlasitis, S., McCubbin, J. A., Yun, J., Widrick, J. J. and Pavol, M. J. (2015). Gait characteristics of adults with Down syndrome explain their greater metabolic rate during walking. *Gait Posture* 41, 180–184.

Alexander, R. M. (1981). Factors of safety in the structure of animals. *Sci. Prog.* 67, 109–130.

Alexander, R. (1988). Symmorphosis and safety factors. In *Principles of Animal Design* (eds. Weibel, D., Taylor, C., and Bolis, L.), pp. 28–35. Cambridge: Cambridge University Press.

Alexander, R. M. (1997). A theory of mixed chains applied to safety factors in biological systems. *J. Theor. Biol.* 184, 247–252.

Allum, J. H. J., Bloem, B. R., Carpenter, M. G., Hulliger, M. and Hadders-Algra, M. (1998). Proprioceptive control of posture: a review of new concepts. *Gait Posture* 8, 214–242.

Alneas, E. (1967). Static and dynamic properties of Golgi tendon organs in the anterior tibial and soleus muscles of the cat. *Acta Physiol. Scand.* 70, 176–187.

Andrada, E., Rode, C., Sutedja, Y., Nyakatura, J. A. and Blickhan, R. (2014a). Trunk orientation causes asymmetries in leg function in small bird terrestrial locomotion. *Proc. Biol. Sci.* 281,.

Andrada, E., Rode, C., Sutedja, Y., Nyakatura, J. A. and Blickhan, R. (2014b). Data from: Trunk orientation causes asymmetries in leg function in small bird terrestrial locomotion. *Dryad Digit. Repos. Httpsdoiorg105061dryadjh5h4*.

Andrada, E., Haase, D., Sutedja, Y., Nyakatura, J. A., Kilbourne, B. M., Denzler, J., Fischer, M. S. and Blickhan, R. (2015). Mixed gaits in small avian terrestrial locomotion. *Sci. Rep.* 5, 13636.

Aoi, S., Katayama, D., Fujiki, S., Tomita, N., Funato, T., Yamashita, T., Senda, K. and Tsuchiya, K. (2013). A stability-based mechanism for hysteresis in the walk–trot transition in quadruped locomotion. *J. R. Soc. Interface* 10, 20120908.

Appelberg, B., Jeneskog, T. and Johansson, H. (1975). Rubrospinal control of static and dynamic fusimotor neurones. *Acta Physiol. Scand.* 95, 431–440.

Armstrong, D. M. and Drew, T. (1985). Forelimb electromyographic responses to motor cortex stimulation during locomotion in the cat. *J. Physiol.* 367, 327–351.

Ausborn, J., Stein, W. and Wolf, H. (2007). Frequency Control of Motor Patterning by Negative Sensory Feedback. *J. Neurosci.* 27, 9319–9328.

Bates, D., Mächler, M., Bolker, B. and Walker, S. (2014). Fitting Linear Mixed-Effects Models using lme4. *ArXiv14065823 Stat*.

Beck, B. R. (2009). Muscle forces or gravity–what predominates mechanical loading on bone? Introduction. *Med Sci Sports Exerc* 41, 2033–6.

Benjamini, Y. and Hochberg, Y. (1995). Controlling the False Discovery Rate: A Practical and Powerful Approach to Multiple Testing. *J. R. Stat. Soc. Ser. B Methodol.* 57, 289–300.

Bertram, J. E. and Biewener, A. A. (1988). Bone curvature: sacrificing strength for load predictability? *J. Theor. Biol.* 131, 75–92.

Biewener, A. A. and Daley, M. A. (2007). Unsteady locomotion: integrating muscle function with whole body dynamics and neuromuscular control. *J. Exp. Biol.* 210, 2949–2960.

Bilo, D., Jahner, A. and Nachtigall, W. (1980). Structure and innervation of wing muscle spindles in the domestic pigeon (*Columba livia* var. *domestica*); a light microscopical study. Zool. *J Anat* 103, 41–61.

Bishop, P. J., Graham, D. F., Lamas, L. P., Hutchinson, J. R., Rubenson, J., Hancock, J. A., Wilson, R. S., Hocknull, S. A., Barrett, R. S., Lloyd, D. G., et al. (2018). The influence of speed and size on avian terrestrial locomotor biomechanics: Predicting locomotion in extinct theropod dinosaurs. *PLOS ONE* 13, e0192172.

Blob, R. W., Espinoza, N. R., Butcher, M. T., Lee, A. H., D'Amico, A. R., Baig, F. and Sheffield, K. M. (2014). Diversity of limb-bone safety factors for locomotion in terrestrial vertebrates: evolution and mixed chains. *Integr. Comp. Biol.* 54, 1058–1071.

Boettiger, C., Coop, G. and Ralph, P. (2012). Is Your Phylogeny Informative? Measuring the Power of Comparative Methods. *Evolution* 66, 2240–2251.

Boggs, D. F. (2002). Interactions between locomotion and ventilation in tetrapods. *Comp. Biochem. Physiol. A. Mol. Integr. Physiol.* 133, 269–288.

Burnham, K. P. and Anderson, D. R. (2001). Kullback-Leibler information as a basis for strong inference in ecological studies. *Wildl. Res.* 28, 111–119.

Butcher, M. T. and Blob, R. W. (2008). Mechanics of limb bone loading during terrestrial locomotion in river cooter turtles (*Pseudemys concinna*). *J. Exp. Biol.* 211, 1186–1186.

Butcher, M. T., White, B. J., Hudzik, N. B., Gosnell, W. C., Parrish, J. H. A. and Blob, R. W. (2011). *In vivo* strains in the femur of the Virginia opossum (*Didelphis virginiana*) during terrestrial locomotion: testing hypotheses of evolutionary shifts in mammalian bone loading and design. *J. Exp. Biol.* 214, 2631–2640.

Butler, A. B. and Hodos, W. (2005). *Comparative vertebrate neuroanatomy: evolution and adaptation*. John Wiley & Sons.

Carrier, D. R. and Farmer, C. G. (2000). The Integration of Ventilation and Locomotion in Archosaurs. *Am. Zool.* 40, 87–100.

Clavel, J., Escarguel, G. and Merceron, G. (2015). mvMORPH: an R package for fitting multivariate evolutionary models to morphometric data. *Methods Ecol. Evol.* 6, 1311–1319.

Cooper, N., Thomas, G. H., Venditti, C., Meade, A. and Freckleton, R. P. (2016). A cautionary note on the use of Ornstein Uhlenbeck models in macroevolutionary studies. *Biol. J. Linn. Soc. Linn. Soc. Lond.* 118, 64–77.

Crago, P. E., Houk, J. C. and Rymer, W. Z. (1982). Sampling of total muscle force by tendon organs. *J. Neurophysiol.* 47, 1069–1083.

Cressler, C. E., Butler, M. A. and King, A. A. (2015). Detecting Adaptive Evolution in Phylogenetic Comparative Analysis Using the Ornstein-Uhlenbeck Model. *Syst. Biol.* 64, 953–968.

Daley, M. A., Usherwood, J. R., Felix, G. and Biewener, A. A. (2006). Running over rough terrain: guinea fowl maintain dynamic stability despite a large unexpected change in substrate height. *J. Exp. Biol.* 209, 171–187.

Daley, M. A., Channon, A. J., Nolan, G. S. and Hall, J. (2016). Preferred gait and walk–run transition speeds in ostriches measured using GPS-IMU sensors. *J. Exp. Biol.* 219, 3301–3308.

Demes, B., Larson, S. G., Stern, J. T., Jungers, W. L., Biknevicius, A. R. and Schmitt, D. (1994). The kinetics of primate quadrupedalism: "hindlimb drive" reconsidered. *J. Hum. Evol.* 26, 353–374.

Drew, T., Jiang, W. and Widajewicz, W. (2002). Contributions of the motor cortex to the control of the hindlimbs during locomotion in the cat. *Brain Res. Rev.* 40, 178–191.

Drew, T., Prentice, S. and Schepens, B. (2004). Cortical and brainstem control of locomotion. *Prog. Brain Res.* 143, 251–61.

English, A. W. (1989). Interlimb Coordination During Locomotion. *Integr. Comp. Biol.* 29, 255–266.

Fabre, A.-C., Granatosky, M. C., Hanna, J. B. and Schmitt, Daniel (2016). Coevolution between forelimb shape and loading regime in strepsirrhines. *Anat. Rec.* S299, 154.

Felsenstein, J. (1985). Phylogenies and the Comparative Method. *Am. Nat.* 125, 1–15.

Fortier, P. A., Smith, A. M. and Rossignol, S. (1987). Locomotor deficits in the mutant mouse, Lurcher. *Exp. Brain Res.* 66, 271–286.

Full, R. J., Kubow, T., Schmitt, J., Holmes, P. and Koditschek, D. (2002). Quantifying dynamic stability and maneuverability in legged locomotion. *Integr. Comp. Biol.* 42, 149–157.

Garland, T., Harvey, P. H. and Ives, A. R. (1992). Procedures for the analysis of comparative data using phylogenetically independent contrasts. *Syst. Biol.* 41, 18–32.

Gintof, C., Konow, N., Ross, C. F. and Sanford, C. P. J. (2010). Rhythmic chewing with oral jaws in teleost fishes: a comparison with amniotes. *J. Exp. Biol.* 213, 1868–1875.

Gosnell, W. C., Butcher, M. T., Maie, T. and Blob, R. W. (2011). Femoral loading mechanics in the Virginia opossum, *Didelphis virginiana*: torsion and mediolateral bending in mammalian locomotion. *J. Exp. Biol.* 214, 3455–3466.

Granatosky, M. C. (2015). Kinetic and kinematic patterns of arm-swinging in the red-shanked douc langur (*Pygathrix nemaeus*). *J. Vietnam. Primatol.* 2, 33–40.

Granatosky, M. C. (2018). Forelimb and hindlimb loading patterns during quadrupedal locomotion in the large flying fox (*Pteropus vampyrus*) and common vampire bat (*Desmodus rotundus*). *J. Zool.* 305, 63–72.

Granatosky, M. C. and Schmitt, D. (2019). The mechanical origins of arm-swinging. *J. Hum. Evol.* 130, 61–71.

Granatosky, M. C., Tripp, C. H. and Schmitt, D. (2016). Gait kinetics of above and below branch quadrupedal locomotion in lemurid primates. *J. Exp. Biol.* 219, 53–63.

Granatosky, M. C., Bryce, C. M., Hanna, J., Fitzsimons, A., Laird, M. F., Stilson, K., Wall, C. E. and Ross, C. F. (2018a). Inter-stride variability triggers gait transitions in mammals and birds. *Proc. R. Soc. B* 285,.

Granatosky, M. C., Fitzsimons, A., Zeininger, A. and Schmitt, D. (2018b). Mechanisms for the functional differentiation of the propulsive and braking roles of the forelimbs and hindlimbs during quadrupedal walking in primates and felines. *J. Exp. Biol.* 221, 1–11.

Gray, J. (1944). Studies in the Mechanics of the Tetrapod Skeleton. *J. Exp. Biol.* 20, 88–116.

Gray, J. (1968). *Animal locomotion*. London: William Clowes and Sons.

Gregory, J. E. and Proske, U. (1975). Responses of tendon organs in a lizard. *J. Physiol.* 248, 519–529.

Gregory, J. E., Brockett, C. L., Morgan, D. L., Whitehead, N. P. and Proske, U. (2002). Effect of eccentric muscle contractions on Golgi tendon organ responses to passive and active tension in the cat. *J. Physiol.* 538, 209–218.

Grillner, S. (1975). Locomotion in vertebrates: central mechanisms and reflex interaction. *Physiol. Rev.* 55, 247–304.

Grillner, S. and Zangger, P. (1979). On the central generation of locomotion in the low spinal cat. *Exp. Brain Res.* 34,.

Grillner, S. and Zangger, P. (1984). The effect of dorsal root transection on the efferent motor pattern in the cat's hindlimb during locomotion. *Acta Physiol. Scand.* 120, 393–405.

Haiden, G. J. and Awad, E. A. (1981). The ultrastructure of the avian Golgi tendon organ. *Anat. Rec.* 200, 153–161.

Hansen, T. F. (1997). Stabilizing selection and the comparative analysis of adaptation. *Evolution* 51, 1341–1351.

Hedges, S. B., Dudley, J. and Kumar, S. (2006). TimeTree: a public knowledge-base of divergence times among organisms. *Bioinforma. Oxf. Engl.* 22, 2971–2972.

Hedges, S. B., Marin, J., Suleski, M., Paymer, M. and Kumar, S. (2015). Tree of Life Reveals Clock-Like Speciation and Diversification. *Mol. Biol. Evol.* 32, 835–845.

Hiiemae, K. M. and Palmer, J. B. (2003). Tongue movements in feeding and speech. *Crit. Rev. Oral Biol. Med.* 14, 413–429.

Hiiemae, K. M., Hayenga, S. M. and Reese, A. (1995). Patterns of tongue and jaw movement in a cinefluorographic study of feeding in the macaque. *Arch. Oral Biol.* 40, 229–246.

Ho, L. si T. and Ané, C. (2014). A linear-time algorithm for Gaussian and non-Gaussian trait evolution models. *Syst. Biol.* 63, 397–408.

Horcholle-Bossavit, G., Jami, L., Petit, J., Vejsada, R. and Zytnicki, D. (1990). Ensemble discharge from Golgi tendon organs of cat peroneus tertius muscle. *J. Neurophysiol.* 64, 813–821.

Houk, J. and Henneman, E. (1967). Responses of Golgi tendon organs to active contractions of the soleus muscle of the cat. *J. Neurophysiol.* 30, 466–481.

Huber, G. C. and Dewitt, L. M. (1900). A contribution on the nerve terminations in neuro-tendinous end-organs. *J. Comp. Neurol.* 10, 159–208.

Hulliger, M. (1984). The mammalian muscle spindle and its central control. In *Reviews of Physiology, Biochemistry and Pharmacology, Volume 101*, pp. 1–110. Springer.

Ichise, T., Kano, M., Hashimoto, K., Yanagihara, D., Nakao, K., Shigemoto, R., Katsuki, M. and Aiba, A. (2000). mGluR1 in cerebellar Purkinje cells essential for long-term depression, synapse elimination, and motor coordination. *Science* 288, 1832–1835.

Ives, A. R., Midford, P. E. and Garland, T. (2007). Within-species variation and measurement error in phylogenetic comparative methods. *Syst. Biol.* 56, 252–270.

James, N. T. and Meek, G. (1973). An electron microscopical study of avian muscle spindles. *J. Ultrastruct. Res.* 43, 193–204.

Jedrzejewski, W., Schmidt, K., Theuerkauf, J., Jedrzejewska, B. and Okarma, H. (2001). Daily movements and territory use by radio-collared wolves (*Canis lupus*) in Bialowieza Primeval Forest in Poland. *Can. J. Zool.* 79, 1993–2004.

Jetz, W. and Pyron, R. A. (2018). The interplay of past diversification and evolutionary isolation with present imperilment across the amphibian tree of life. *Nat. Ecol. Evol.* 2, 850.

Jetz, W., Thomas, G. H., Joy, J. B., Redding, D. W., Hartmann, K. and Mooers, A. O. (2014). Global distribution and conservation of evolutionary distinctness in birds. *Curr. Biol. CB* 24, 919–930.

Johansson, H. (1988). Rubrospinal and rubrobulbospinal influences on dynamic and static gamma-motoneurones. *Behav. Brain Res.* 28, 97–107.

Jordan, K., Challis, J. H. and Newell, K. M. (2007). Walking speed influences on gait cycle variability. *Gait Posture* 26, 128–134.

Karakasiliotis, K., Thandiackal, R., Melo, K., Horvat, T., Mahabadi, N. K., Tsitkov, S., Cabelguen, J. M. and Ijspeert, A. J. (2016). From cineradiography to biorobots: an approach for designing robots to emulate and study animal locomotion. *J. R. Soc. Interface* 13,.

Keene, O. N. (1995). The log transformation is special. *Stat. Med.* 14, 811–819.

Kilbourne, B. M., Andrada, E., Fischer, M. S. and Nyakatura, J. A. (2016). Morphology and motion: hindlimb proportions and swing phase kinematics in terrestrially locomoting charadriiform birds. *J. Exp. Biol.* 219, 1405–1416.

Klaassen, R. H., Strandberg, R., Hake, M. and Alerstam, T. (2008). Flexibility in daily travel routines causes regional variation in bird migration speed. *Behav. Ecol. Sociobiol.* 62, 1427–1432.

Knight, K. C. and Lee, D. (2019). Comparative biomechanics of horizontal, fine-branch locomotion in lizards: Part 1. In *Integrative and Comparative Biology*, p. E125. Tampa Florida: Integrative and Comparative Biology.

Kram, R. and Taylor, C. R. (1990). Energetics of running: a new perspective. *Nature* 346, 265.

Kuhn, T. S., Mooers, A. Ø. and Thomas, G. H. (2011). A simple polytomy resolver for dated phylogenies. *Methods Ecol. Evol.* 2, 427–436.

Kumar, S. and Hedges, S. B. (2011). TimeTree2: species divergence times on the iPhone. *Bioinforma. Oxf. Engl.* 27, 2023–2024.

Kumar, S., Stecher, G., Suleski, M. and Hedges, S. B. (2017). TimeTree: A Resource for Timelines, Timetrees, and Divergence Times. *Mol. Biol. Evol.* 34, 1812–1819.

Lowell, R. B. (1985). Selection for increased safety factors of biological structures as environmental unpredictability increases. *Science* 228, 1009–1011.

Maier, A. (1992). The avian muscle spindle. *Anat. Embryol. (Berl.)* 186, 1–25.

Marcus Rowcliffe, J., Carbone, C., Kays, R., Kranstauber, B. and Jansen, P. A. (2012). Bias in estimating animal travel distance: the effect of sampling frequency. *Methods Ecol. Evol.* 3, 653–662.

Matthews, P. B. (1972). Mammalian muscle receptors and their central actions.

McElroy, E. J., Wilson, R., Biknevicius, A. R. and Reilly, S. M. (2014). A comparative study of single-leg ground reaction forces in running lizards. *J. Exp. Biol.* 217, 735–742.

Mileusnic, M. P. and Loeb, G. E. (2009). Force estimation from ensembles of Golgi tendon organs. *J. Neural Eng.* 6, 036001.

Morton, S. M. and Bastian, A. J. (2006). Cerebellar contributions to locomotor adaptations during splitbelt treadmill walking. *J. Neurosci. Off. J. Soc. Neurosci.* 26, 9107–9116.

Munteanu, V., Diamond, K., Schneider, N., Riley, A., McKamy, A. and Blob, R. W. (2019). Effects of Ecological Transitions on Locomotor Morphology: Do Changes in Bone Loads Have Implications for Limb Elongation in Arboreal Tetrapods? p. 374. Tampa Florida: Integrative and Comparative Biology.

Nagy, K. A. (1987). Field metabolic rate and food requirement scaling in mammals and birds. *Ecol. Monogr.* 57, 111–128.

Nagy, K. A. (2005). Field metabolic rate and body size. *J. Exp. Biol.* 208, 1621–1625.

Nagy, K. A., Girard, I. A. and Brown, T. K. (1999). Energetics of Free-Ranging Mammals, Reptiles, and Birds. *Annu. Rev. Nutr.* 19, 247–277.

Nassar, P. N., Jackson, A. C. and Carrier, D. R. (2001). Entraining the natural frequencies of running and breathing in guinea fowl (*Numida meleagris*). *J. Exp. Biol.* 204, 1641–1651.

Nyakatura, J. A., Andrada, E., Curth, S. and Fischer, M. S. (2014). Bridging "Romer's Gap": Limb Mechanics of an Extant Belly-Dragging Lizard Inform Debate on Tetrapod Locomotion During the Early Carboniferous. *Evol. Biol.* 41, 175–190.

Nyakatura, J. A., Melo, K., Horvat, T., Karakasiliotis, K., Allen, V. R., Andikfar, A., Andrada, E., Arnold, P., Lauströer, J., Hutchinson, J. R., et al. (2019). Reverse-engineering the locomotion of a stem amniote. *Nature* 565, 351.

O'Connor, S. M., Xu, H. Z. and Kuo, A. D. (2012). Energetic cost of walking with increased step variability. *Gait Posture* 36, 102–107.

Ovalle, W. K. (1976). Fine structure of the avian muscle spindle capsule. *Cell Tissue Res.* 166, 285–298.

Palmer, J. B., Hiiemae, K. M. and Liu, J. (1997). Tongue-jaw linkages in human feeding: a preliminary videofluorographic study. *Arch. Oral Biol.* 42, 429–441.

Paradis, E., Claude, J. and Strimmer, K. (2004). APE: Analyses of Phylogenetics and Evolution in R language. *Bioinformatics* 20, 289–290.

Pearson, K. G., Misiaszek, J. E. and Fouad, K. (1998). Enhancement and Resetting of Locomotor Activity by Muscle Afferents. *Ann. N. Y. Acad. Sci.* 860, 203–215.

Pontzer, H. (2016). A unified theory for the energy cost of legged locomotion. *Biol. Lett.* 12, 20150935.

Prochazka, A., Gritsenko, V. and Yakovenko, S. (2002). Sensory control of locomotion: reflexes versus higher-level control. In *Sensorimotor control of movement and posture*, pp. 357–367. Springer.

Proske, U. (1979). The Golgi tendon organ. *Trends Neurosci.* 2, 7–8.

Proske, U. (1997). The mammalian muscle spindle. *Physiology* 12, 37–42.

Purves, D. A. and Fitzpatrick, G. (2001). *Neuroscience*. Sunderland, MA: Sinauer Associates Inc.

Reilly, S. M., McElroy, E. J. and Biknevicius, A. R. (2007). Posture, gait and the ecological relevance of locomotor costs and energy-saving mechanisms in tetrapods. *Zoology* 110, 271–289.

Revell, L. J. (2012). phytools: an R package for phylogenetic comparative biology (and other things). *Methods Ecol. Evol.* 3, 217–223.

Riemann, B. L. and Lephart, S. M. (2002). The sensorimotor system, part II: the role of proprioception in motor control and functional joint stability. *J. Athl. Train.* 37, 80.

Romanovsky, D., Moseley, A. E., Mrak, R. E., Taylor, M. D. and Dobretsov, M. (2007). Phylogenetic preservation of α3 Na+, K+-ATPase distribution in vertebrate peripheral nervous systems. *J. Comp. Neurol.* 500, 1106–1116.

Roquet, C., Lavergne, S. and Thuiller, W. (2014). One tree to link them all: a phylogenetic dataset for the European tetrapoda. *PLoS Curr.* 6,.

Ross, C. F., Eckhardt, A., Herrel, A., Hylander, W. L., Metzger, K. A., Schaerlaeken, V., Washington, R. L. and Williams, S. H. (2007). Modulation of intra-oral processing in mammals and lepidosaurs. *Integr. Comp. Biol.* 47, 118–136.

Ross, C. F., Baden, A. L., Georgi, J., Herrel, A., Metzger, K. A., Reed, D. A., Schaerlaeken, V. and Wolff, M. S. (2010). Chewing variation in lepidosaurs and primates. *J. Exp. Biol.* 213, 572–584.

Ross, C. F., Blob, R. W., Carrier, D. R., Daley, M. A., Deban, S. M., Demes, B., Gripper, J. L., Iriarte-Diaz, J., Kilbourne, B. M., Landberg, T., et al. (2013). The Evolution of Locomotor Rhythmicity in Tetrapods. *Evolution* 67, 1209–1217.

Schliep, K. P. (2011). phangorn: phylogenetic analysis in R. *Bioinforma. Oxf. Engl.* 27, 592–593.

Schmitt, D. (1999). Compliant walking in primates. *J. Zool.* 248, 149–160.

Schmitt, D. and Hanna, J. B. (2004). Substrate alters forelimb to hindlimb peak force ratios in primates. *J. Hum. Evol.* 46, 239–54.

Schmitz, L. and Higham, T. E. (2018). Non-uniform evolutionary response of gecko eye size to changes in diel activity patterns. *Biol. Lett.* 14, 20180064.

Serrien, D. J., Li, Y., Steyvers, M., Debaere, F. and Swinnen, S. P. (2001). Proprioceptive regulation of interlimb behavior: interference between passive movement and active coordination dynamics. *Exp. Brain Res.* 140, 411–419.

Sheffield, K. M. and Blob, R. W. (2011). Loading mechanics of the femur in tiger salamanders (*Ambystoma tigrinum*) during terrestrial locomotion. *J. Exp. Biol.* 214, 2603–2615.

Sheffield, K. M., Butcher, M. T., Shugart, S. K., Gander, J. C. and Blob, R. W. (2011). Locomotor loading mechanics in the hindlimbs of tegu lizards (*Tupinambis merianae*): comparative and evolutionary implications. *J. Exp. Biol.* 214, 2616–2630.

Shneider, N. A., Brown, M. N., Smith, C. A., Pickel, J. and Alvarez, F. J. (2009). Gamma motor neurons express distinct genetic markers at birth and require muscle spindle-derived GDNF for postnatal survival. *Neural Develop.* 4, 42.

Sokal, R. R. and Rohlf, F. J. (2012). *Biometry : the principles and practice of statistics in biological research*. 6th ed. New York: Freeman & Company.

Stark, R. C., Fox, S. F. and Leslie Jr, D. M. (2005). Male Texas horned lizards increase daily movements and area covered in spring: a mate searching strategy? *J. Herpetol.* 39, 169–173.

Taylor, C. R., Heglund, N. C., McMAHON, T. A. and Looney, T. R. (1980). Energetic cost of generating muscular force during running: a comparison of large and small animals. *J. Exp. Biol.* 86, 9–18.

Taylor, C. R., Heglund, N. C. and Maloiy, G. M. (1982). Energetics and mechanics of terrestrial locomotion. I. Metabolic energy consumption as a function of speed and body size in birds and mammals. *J. Exp. Biol.* 97, 1–21.

ten Donkelaar, H. J. (1988). Evolution of the red nucleus and rubrospinal tract. *Behav. Brain Res.* 28, 9–20.

Thompson, G. (1992). Daily distance travelled and foraging areas of Varanus gouldii (Reptilia: Varanidae) in a semi-urban environment. *Wildl. Res.* 19, 743–753.

Thompson, G. G., De Boer, M. and Pianka, E. R. (1999). Activity areas and daily movements of an arboreal monitor lizard, Varanus tristis (Squamata: Varanidae) during the breeding season. *Aust. J. Ecol.* 24, 117–122.

Tonini, J. F. R., Beard, K. H., Ferreira, R. B., Jetz, W. and Pyron, R. A. (2016). Fully-sampled phylogenies of squamates reveal evolutionary patterns in threat status. *Biol. Conserv.* 204, 23–31.

Verdaasdonk, B. W., Koopman, H. F. J. M. and Helm, F. C. T. V. D. (2006). Energy efficient and robust rhythmic limb movement by central pattern generators. *Neural Netw.* 19, 388–400.

Wetzel, M. C., Atwater, A. E., Wait, J. V. and Stuart, D. G. (1976). Kinematics of locomotion by cats with a single hindlimb deafferented. *J. Neurophysiol.* 39, 667–678.

Wild, J. M. and Williams, M. N. (2000). Rostral wulst in passerine birds. I. Origin, course, and terminations of an avian pyramidal tract. *J. Comp. Neurol.* 416, 429–450.

Winter, B. (2013). Linear models and linear mixed effects models in R with linguistic applications. *ArXiv13085499 Cs*.

Yanagihara, D., Udo, M., Kondo, I. and Yoshida, T. (1993). A new learning paradigm: adaptive changes in interlimb coordination during perturbed locomotion in decerebrate cats. *Neurosci. Res.* 18, 241–244.

Figures

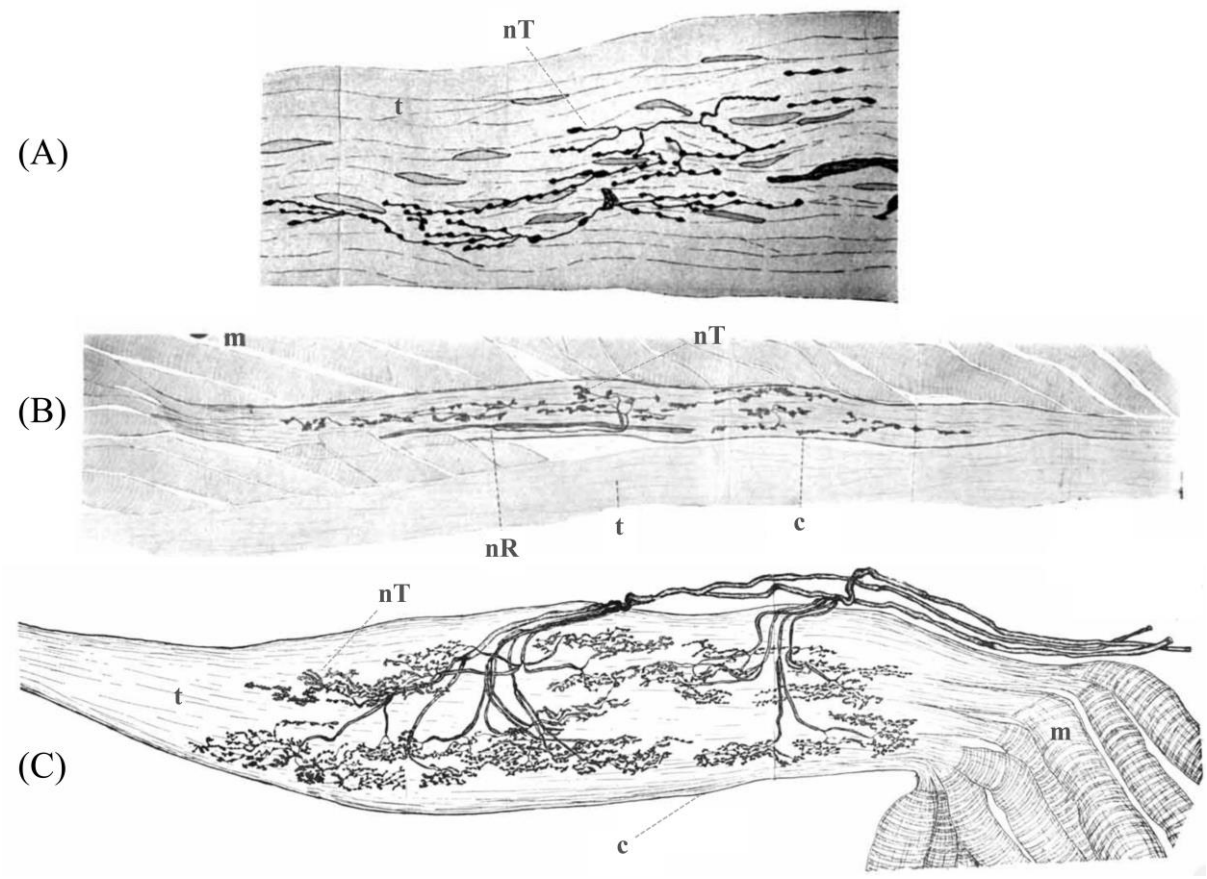

Figure 1: Histological preparations of the Golgi tendon organs from an (A) amphibian, (B) bird, (C) and mammal. Representative histological sections were prepared specifically from *m. tibialis posterior* of a frog, an undisclosed wing muscle of a dove, and an undisclosed hindlimb muscle of a rabbit. *nT* = Terminations of nerve fibers; *t* = tendon; *m* = striated muscle fibers; *nR*= nodes of Ranvier; *c*= capsule of neuro-tendinous end organs. Figures adapted from Huber and Dewitt (1900) with permission. All information about histological preparation and imaging is available in Huber and Dewitt (1900).

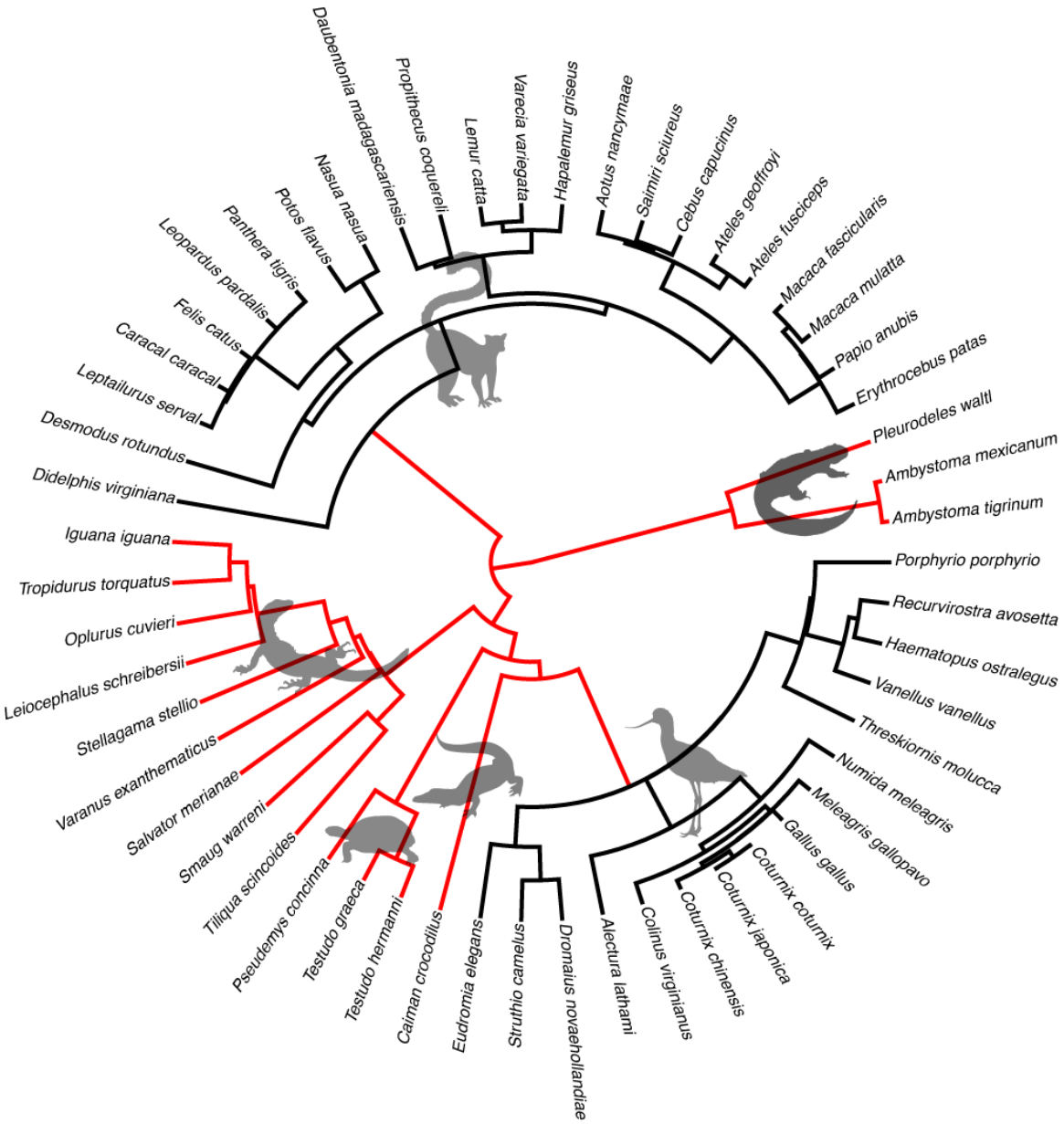

Figure 2: Phylogeny of species used in this study. Branch colors on phylogeny correspond to hypothesized ancestral Golgi tendon organ morphology (encapsulated = black, unencapsulated = red). Silhouette figures were acquired from *PhyloPic* and original figures were made available by: Avocet: Alexander Vong CC BY 3.0, Salamander: Matt Reinbold (modified by T. Michael Keesey) CC BY-SA 3.0, Turtle: Andrew A. Farke CC BY 3.0, Lemur: Roberto Díaz Sibaja CC BY 3.0.

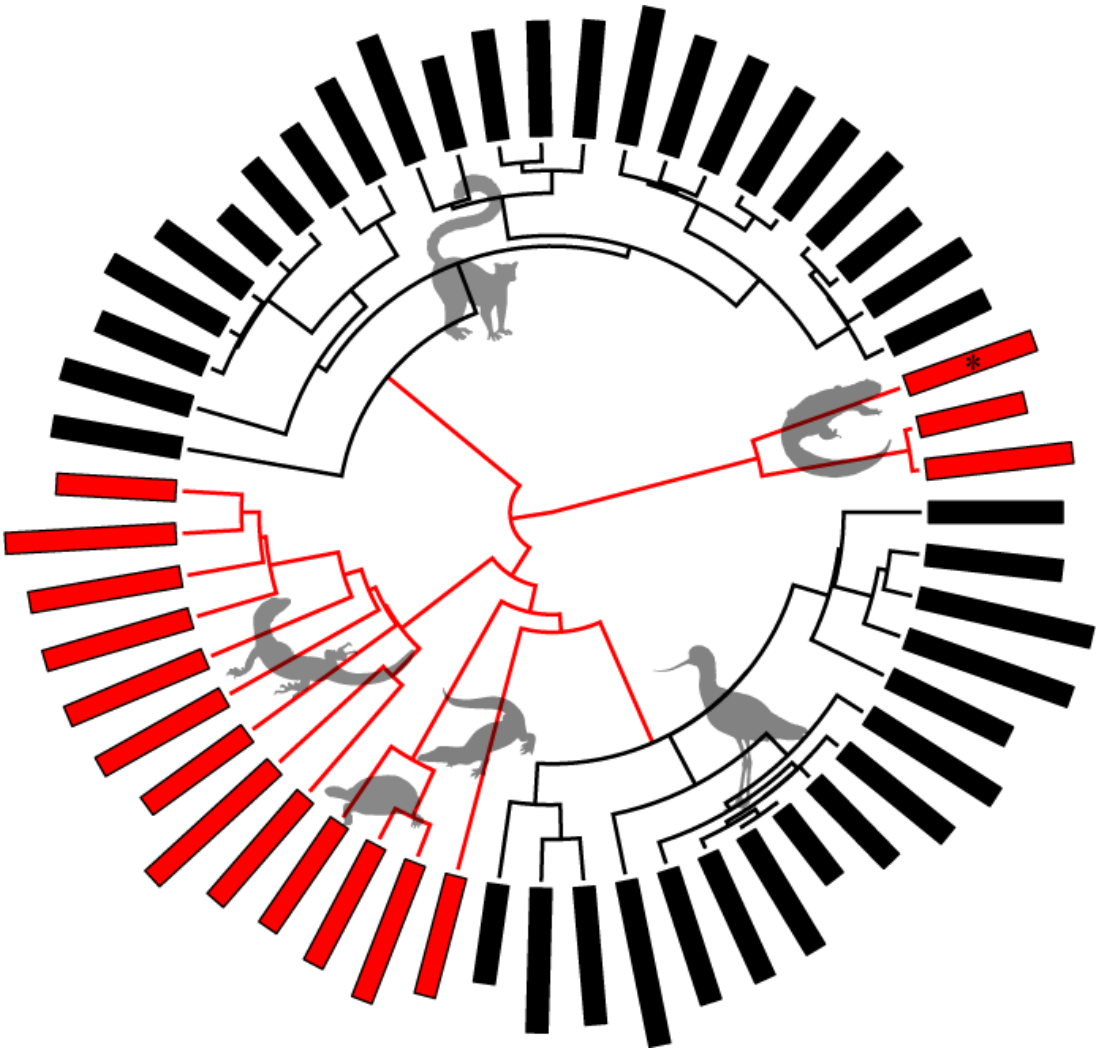

Figure 3: Phylogeny of species used in this study and bar graphs of log-transformed mean coefficients of variation (CV^*) of stride cycle duration for each species. Use Figure 2 as a reference for all scientific names. Coefficients of variation were calculated within individuals for each species using $CV^* = \left(1 + \frac{1}{4n}\right) CV$, where *n* is equal to the number of strides. Species with encapsulated Golgi tendon organs (GTO) are illustrated in black and species with unencapsulated GTOs are in red. Branch colors on phylogeny correspond to hypothesized ancestral GTO morphology (encapsulated = black, unencapsulated = red). For scale use *Pleurodeles waltl* (marked with an *) at 1.32.

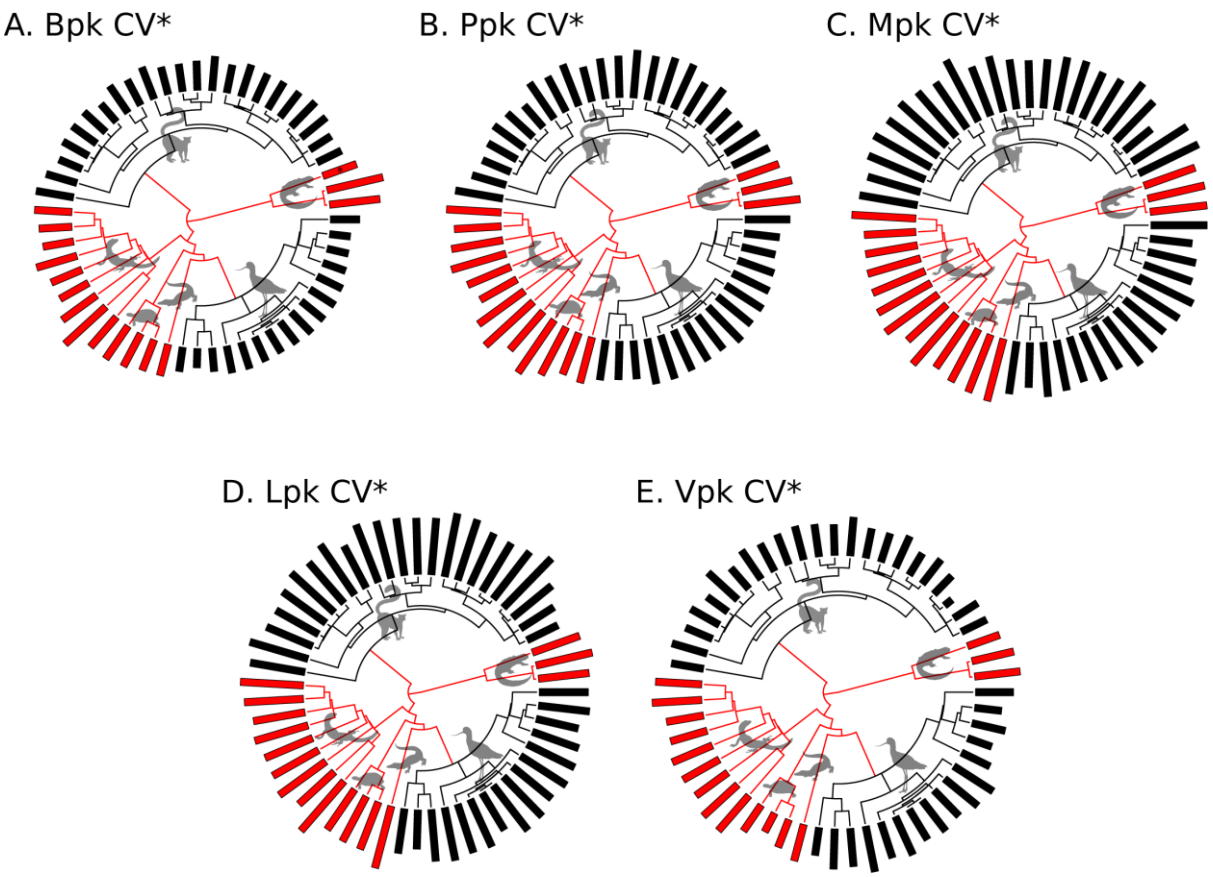

Figure 4: Phylogeny of species used in this study and bar graphs of log-transformed mean coefficients of variation (CV^*) of (A) braking peak, (B) propulsive peak, (C) medial peak, (D) lateral peak, and (E) vertical peak force for each species. Use Figure 2 as a reference for all scientific names. Coefficients of variation were calculated within individuals for each species using $CV^* = \left(1 + \frac{1}{4n}\right) CV$, where *n* is equal to the number of strides. Species with encapsulated Golgi tendon organs (GTO) are illustrated in black and species with unencapsulated GTOs are in red. Branch colors on phylogeny correspond to hypothesized ancestral GTO morphology (encapsulated = black, unencapsulated = red). For scale use braking peak CV^* for *Pleurodeles waltl* (marked with an *) at 1.92.

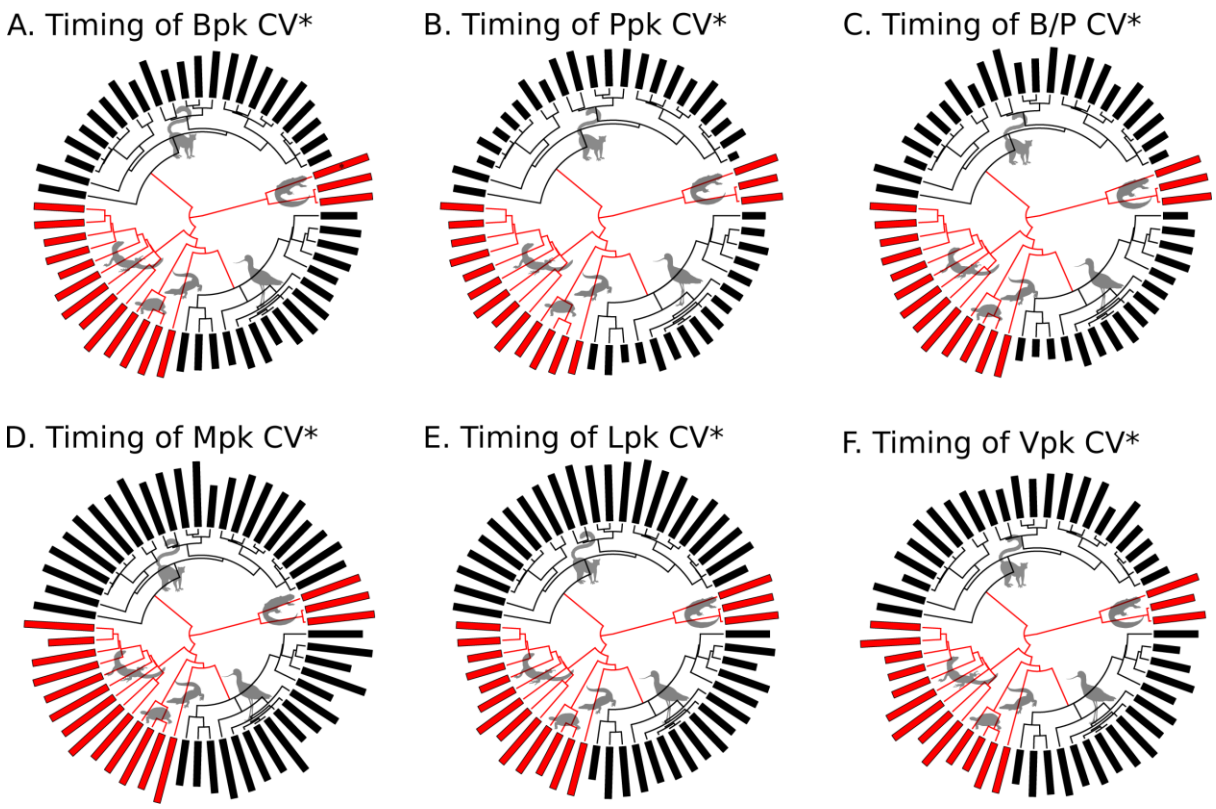

Figure 5: Phylogeny of species used in this study and bar graphs of log-transformed mean coefficients of variation (CV^*) of the timing of (A) braking peak, (B) braking to propulsive transition, (C) propulsive peak, (D) medial peak, (E) lateral peak, and (F) vertical peak force for each species. Use Figure 2 as a reference for all scientific names. Coefficients of variation were calculated within individuals for each species using $CV^* = \left(1 + \frac{1}{4n}\right) CV$, where *n* is equal to the number of strides. Species with encapsulated Golgi tendon organs (GTO) are illustrated in black and species with unencapsulated GTOs are in red. Branch colors on phylogeny correspond to hypothesized ancestral GTO morphology (encapsulated = black, unencapsulated = red). For scale use timing of braking peak CV^* for *Pleurodeles waltl* (marked with an *) at 2.21.

Tables:

Table 1: Coefficients of variation (CV^*) (mean ± standard deviation) for limb loading magnitude for each of the study species.

Species	Golgi tendon organ morphology	Peak braking force CV^*	Peak propulsive force CV^*	Peak medial force CV^*	Peak lateral force CV^*	Peak vertical force CV^*
Testudo hermanni	Unencapsulated	58.75	35.05	83.00	33.74	9.45
Tiliqua scincoides	Unencapsulated	134.75	57.51	114.88	94.29	33.71
Caiman crocodilus	Unencapsulated	55.57 ± 26.57	43.82 ± 4.52	99.90 ± 9.87	84.34 ± 8.90	17.31 ± 5.43
Smaug warreni	Unencapsulated	940.74 ± 18.99	178.45 ± 145.37	43.86 ± 8.49	27.51 ± 26.16	33.84 ± 6.92
Iguana iguana	Unencapsulated	104.95 ± 6.07	81.04 ± 26.11	99.21 ± 38.17	79.57 ± 3.03	33.46 ± 3.72
Stellagama st ellio	Unencapsulated	61.50 ± 46.16	41.79 ± 9.45	57.75 ± 24.88	35.26 ± 22.95	26.68 ± 7.91
Leiocephalus schreibersi	Unencapsulated	184.43 ± 183.35	94.49 ± 27.70	51.00 ± 31.73	46.30 ± 15.02	17.83 ± 5.66
Tropidurus torquatus	Unencapsulated	60.19 ± 16.50	43.18 ± 22.83	40.55 ± 45.86	60.42 ± 48.16	43.01 ± 10.23
Varanus exanthematicus	Unencapsulated	56.84 ± 20.45	28.40 ± 14.67	77.38 ± 45.39	37.48 ± 21.37	23.08 ± 8.73
Oplurus cuvieri	Unencapsulated	47.20 ± 17.48	64.38 ± 16.67	43.07 ± 6.41	37.41 ± 10.57	17.22 ± 11.82
Pleurodeles waltl	Unencapsulated	84.01	31.81	47.75	32.10	12.97
Pseudemys concinna	Unencapsulated	139.27 ± 47.59	168.18 ± 25.78	51.35 ± 7.41	28.93 ± 7.51	10.77 ± 4.15
Salvator merianae	Unencapsulated	184.38 ± 83.09	92.23 ± 33.49	102.16 ± 56.64	53.07 ± 31.07	19.52 ± 7.89
Ambystoma mexicanum	Unencapsulated	1241.07 ± 2041.47	60.34 ± 43.79	64.48 ± 16.87	53.65 ± 9.19	25.55 ± 4.18

Testudo graeca	Unencapsulated	99.37 ± 73.59	74.14 ± 88.58	69.75 ± 7.31	33.82 ± 5.60	4.93 ± 2.51
Ambystoma tigrinum	Unencapsulated	547.55 ± 822.33	91.18 ± 24.26	60.02 ± 18.48	34.34 ± 9.20	32.16 ± 6.89
Ateles fusciceps	Encapsulated	50.02	31.03	84.04	61.64	10.20
Ateles geoffroyi	Encapsulated	48.21	19.61	42.53	49.23	6.79
Erythrocebus patas	Encapsulated	28.09	25.76	113.38	10.64	8.25
Leopardus pardalis	Encapsulated	39.50	16.66	93.11	57.25	20.67
Papio anubis	Encapsulated	22.53	22.48	103.81	15.51	8.38
Alectura lathami	Encapsulated	30.48 ± 9.81	39.81 ± 1.97	38.81 ± 5.64	42.05 ± 0.75	33.77 ± 1.45
Caracal caracal	Encapsulated	37.58 ± 5.53	14.11 ± 10.70	105.34 ± 14.39	29.26 ± 6.56	11.81 ± 7.26
Coturnix coturnix	Encapsulated	30.08 ± 2.72	29.33 ± 3.07	64.93 ± 3.47	50.49 ± 0.05	18.55 ± 1.30
Eudromia elegans	Encapsulated	21.18 ± 8.67	25.65 ± 10.93	44.40 ± 7.15	22.79 ± 5.07	8.45 ± 6.93
Felis catus	Encapsulated	39.75 ± 4.50	20.27 ± 18.20	84.12 ± 19.14	39.92 ± 6.40	6.86 ± 0.02
Hapalemur griseus	Encapsulated	73.51 ± 7.53	47.05 ± 20.91	33.55 ± 5.81	51.31 ± 34.96	19.03 ± 8.29
Leptailurus serval	Encapsulated	21.80 ± 1.76	11.46 ± 7.12	80.81 ± 18.98	31.66 ± 2.91	8.96 ± 4.58
Macaca fasicularis	Encapsulated	72.64 ± 10.59	11.33 ± 2.34	50.67 ± 2.51	116.43 ± 2.32	6.85 ± 3.21
Macaca mulatta	Encapsulated	53.18 ± 22.92	10.95 ± 6.73	11.93 ± 11.52	32.95 ± 8.62	2.04 ± 2.39
Nasua nasua	Encapsulated	35.09 ± 7.72	23.55 ± 3.56	140.78 ± 31.49	26.92 ± 8.00	10.36 ± 5.94
Potos flavus	Encapsulated	57.58 ± 1.39	32.60 ± 0.90	52.69 ± 41.56	67.52 ± 3.98	13.97 ± 8.43
Recurvirostra avosetta	Encapsulated	13.56 ± 1.28	17.20 ± 13.94	20.70 ± 2.44	35.26 ± 16.02	7.84 ± 3.44

Struthio camelus	Encapsulated	11.08 ±0.85	22.17 ± 10.43	25.05 ± 2.82	15.21 ± 16.48	21.28 ± 3.24
Threskiornis molucca	Encapsulated	31.76 ± 13.51	25.68 ± 7.56	73.92 ± 27.05	38.77 ± 24.49	10.95 ± 3.49
Aotus nancymaae	Encapsulated	34.27 ± 10.97	35.70 ± 3.75	47.46 ± 9.24	87.23 ± 14.91	9.82 ± 1.72
Cebus capucinus	Encapsulated	45.11 ± 10.81	47.97 ± 17.67	37.12 ± 13.65	51.16 ± 31.24	13.77 ± 7.33
Daubentonia madagascariensis	Encapsulated	69.01 ± 18.32	34.67 ± 10.59	42.52 ± 3.08	72.70 ± 17.61	11.73 ± 2.41
Desmodus rotundus	Encapsulated	53.32 ± 72.66	16.79 ± 15.65	50.73 ± 54.29	66.37 ± 35.30	15.92 ± 15.25
Gallus gallus	Encapsulated	36.91 ± 13.54	45.00 ± 16.00	58.23 ± 22.79	46.15 ± 7.64	15.08 ±5.72
Lemur catta	Encapsulated	31.56 ± 5.16	25.92 ± 4.50	35.57 ± 6.59	54.78 ± 16.63	11.94 ± 5.41
Numida meleagris	Encapsulated	39.16 ± 8.68	33.07 ± 7.96	51.27 ± 12.78	43.16 ± 14.31	34.26 ± 12.29
Porphyrio porphyrio	Encapsulated	38.44 ± 5.10	36.99 ± 0.83	56.29 ± 20.85	30.01 ± 3.42	17.93 ± 8.60
Propithecus coquereli	Encapsulated	33.67 ± 8.35	17.42 ± 13.40	59.46 ± 10.55	59.68 ± 32.78	13.92 ± 7.48
Varecia variegata	Encapsulated	38.65 ± 14.28	28.47 ± 4.38	29.86 ± 6.69	49.66 ± 12.59	10.47 ± 0.66
Coturnix japonica	Encapsulated	26.24 ± 12.01	30.92 ± 10.89	35.10 ± 23.87	19.89 ± 19.87	14.61 ± 9.19
Haematopus ostralegus	Encapsulated	15.18 ± 5.87	15.46 ± 10.84	33.70 ± 42.51	19.98 ± 15.42	13.29 ± 1.63
Panthera tigris	Encapsulated	18.47 ± 11.12	10.14 ± 5.39	67.57 ± 23.47	41.36 ± 8.26	7.93 ± 2.02
Vanellus vanellus	Encapsulated	19.91 ± 10.64	21.12 ± 15.87	37.60 ± 36.29	29.95 ± 18.52	6.94 ± 4.34
Colinus virginianus	Encapsulated	32.07 ± 12.38	38.92 ± 9.44	28.83 ± 14.06	34.27 ± 14.38	17.14 ± 3.89
Coturnix chinensis	Encapsulated	27.80 ± 4.87	34.18 ± 4.48	44.82 ± 8.68	37.08 ± 10.28	24.19 ± 2.35

Didelphis virginiana	Encapsulated	112.84 ± 114.24	46.93 ± 11.08	66.67 ± 40.42	46.58 ± 6.83	11.87 ± 7.43
Meleagris gallopavo	Encapsulated	37.57 ± 16.00	32.85 ± 9.66	40.06 ± 18.83	32.69 ± 9.31	25.52 ± 6.42
Dromaius novaehollandiae	Encapsulated	18.68 ± 3.26	21.64 ± 3.43	50.23 ± 10.52	36.64 ± 6.31	18.25 ± 3.51
Saimiri sciureus	Encapsulated	63.57 ± 13.42	46.34 ± 7.95	50.82 ± 19.21	82.41 ± 32.02	9.80 ± 1.99

Table 2. Coefficients of variation (CV^*) (mean ± standard deviation) for the timing of peak forces and the braking to propulsive transition for each of the study species.

Species	Golgi tendon organ morphology	Timing of peak braking force CV^*	Timing of braking to propulsive transition CV^*	Timing of peak propulsive force CV^*	Timing of peak medial force CV^*	Timing of peak lateral force CV^*	Timing of peak vertical force CV^*
Testudo hermanni	Unencapsulated	94.74	63.66	35.88	68.48	68.21	40.52
Tiliqua scincoides	Unencapsulated	182.84	149.87	76.13	61.99	98.41	71.27
Caiman crocodilus	Unencapsulated	71.00 ± 5.98	53.38 ± 11.34	21.33 ± 4.69	123.52 ± 3.07	71.45 ± 13.06	37.69 ± 13.47
Smaug warreni	Unencapsulated	59.53	69.72 ± 9.33	18.04 ± 4.30	153.74 ± 57.72	28.42 ± 16.07	24.96 ± 8.87
Iguana iguana	Unencapsulated	85.99 ± 6.15	75.78 ± 27.38	50.80 ± 7.92	154.21 ± 44.40	33.23 ± 19.82	47.40 ± 27.24
Stellagama stellio	Unencapsulated	26.71 ± 24.26	31.81 ± 4.16	18.38 ± 13.89	86.99 ± 55.63	12.02 ± 5.12	21.33 ± 19.24
Leiocephalus schreibersi	Unencapsulated	49.88 ± 28.84	44.60 ± 27.68	37.16 ± 8.21	127.33 ± 39.95	23.00 ± 0.93	18.31 ± 2.47
Tropidurus torquatus	Unencapsulated	82.52 ± 29.45	47.80 ± 10.33	23.74 ±19.52	26.85 ± 28.48	29.58 ± 10.46	102.35 ± 25.68
Varanus exanthematicus	Unencapsulated	79.00 ± 11.25	48.29 ± 4.85	25.00 ± 9.65	109.93 ± 3.95	25.23 ± 23.46	69.25 ± 51.27
Oplurus cuvieri	Unencapsulated	41.77 ± 5.90	34.99 ± 3.04	22.31 ± 4.93	99.89 ± 11.85	15.30 ± 5.04	17.61 ± 7.11
Pleurodeles waltl	Unencapsulated	162.83	76.71	57.89	80.90	79.79	64.44
Pseudemys concinna	Unencapsulated	94.41 ± 33.77	67.56 ± 26.53	36.37 ± 6.62	71.63 ± 38.31	75.90 ± 37.12	21.16 ± 2.68
Salvator merianae	Unencapsulated	113.59 ± 33.76	77.37 ± 9.08	39.52 ± 2.15	92.89 ± 12.69	70.82 ± 33.65	105.53 ± 28.90
Ambystoma mexicanum	Unencapsulated	131.16 ± 32.84	93.65 ± 65.45	34.96 ± 4.75	106.90 ± 27.03	60.47 ± 27.49	31.22 ± 9.43
Testudo graeca	Unencapsulated	101.72 ± 33.54	44.61 ± 18.79	48.76 ± 16.57	88.01 ± 29.06	38.56 ±12.46	17.19 ± 2.96
Ambystoma tigrinum	Unencapsulated	107.24 ± 24.05	99.30 ± 26.26	42.63 ± 4.39	126.52 ± 31.45	71.35 ± 15.67	57.74 ± 14.02
Ateles fusciceps	Encapsulated	72.71	50.34	33.18	71.43	79.42	41.07
Ateles geoffroyi	Encapsulated	38.04	13.46	13.20	58.88	41.04	9.86

Erythrocebus patas	Encapsulated	8.35	5.67	2.38	45.42	18.01	9.57
Leopardus pardalis	Encapsulated	22.34	12.21	6.11	103.93	78.02	42.20
Papio anubis	Encapsulated	12.30	12.69	10.94	65.95	64.22	7.39
Alectura lathami	Encapsulated	19.39 ± 4.08	9.54 ± 3.96	6.69 ± 2.67	76.44 ± 13.98	45.34 ± 1.63	39.43 ± 8.30
Caracal caracal	Encapsulated	29.21 ± 9.66	21.22 ± 3.43	9.56 ± 7.53	112.18 ± 89.70	65.29 ± 17.16	32.52 ± 16.48
Coturnix coturnix	Encapsulated	40.11 ± 8.21	25.12 ± 3.52	15.65 ± 1.92	105.90 ± 9.49	32.19 ± 2.24	42.24 ± 3.72
Eudromia elegans	Encapsulated	30.48 ± 3.87	8.21 ± 1.51	10.01 ± 10.12	26.34 ± 17.11	14.90 ± 2.62	14.23 ± 6.34
Felis catus	Encapsulated	16.73 ± 0.68	15.19 ± 2.51	4.52 ± 1.01	84.85 ± 37.73	58.45 ± 15.69	24.26 ± 2.75
Hapalemur griseus	Encapsulated	60.15 ± 28.33	67.60 ± 6.47	30.27 ± 0.65	19.97 ± 2.97	115.23 ± 19.43	29.07 ± 25.06
Leptailurus serval	Encapsulated	13.48 ± 5.73	7.93 ± 3.23	4.60 ± 2.66	96.95 ± 34.14	81.35 ± 18.95	8.96 ± 4.58
Macaca fasicularis	Encapsulated	32.80 ± 5.00	29.90 ± 1.71	15.42 ± 4.01	32.72 ± 1.50	57.21 ± 4.00	11.49 ± 1.41
Macaca mulatta	Encapsulated	17.25 ± 11.15	24.63 ± 0.19	6.75 ± 6.58	45.17 ± 17.65	60.61 ± 32.87	9.89 ± 4.73
Nasua nasua	Encapsulated	19.00 ± 3.60	9.39 ± 1.98	7.87 ± 1.49	123.55 ± 12.90	74.37 ± 10.85	28.25 ± 12.32
Potos flavus	Encapsulated	46.44 ± 0.04	39.86 ± 2.62	20.36 ± 8.17	71.57 ± 24.05	64.36 ± 4.13	28.30 ± 8.09
Recurvirostra avosetta	Encapsulated	37.59 ± 8.08	20.17 ± 2.95	7.94 ± 4.08	107.61 ± 18.01	53.83 ± 8.03	7.84 ± 3.44
Struthio camelus	Encapsulated	24.12 ± 4.89	5.05 ± 4.87	14.61 ± 4.33	25.71 ± 22.90	61.76 ± 81.02	34.03 ± 1.49
Threskiornis molucca	Encapsulated	15.95 ± 8.66	11.71 ± 0.31	8.80 ± 0.42	16.06 ± 7.88	43.70 ± 17.70	16.56 ± 0.49
Aotus nancymaae	Encapsulated	61.85 ± 36.33	43.22 ± 18.05	24.54 ± 13.49	41.28 ± 7.83	168.45 ± 52.59	36.84 ± 13.57
Cebus capucinus	Encapsulated	48.30 ± 7.04	48.94 ± 17.81	22.74 ± 11.62	64.15 ± 15.43	113.17 ± 32.00	43.55 ± 10.11
Daubentonia madagascariensis	Encapsulated	64.09 ± 1.85	44.20 ± 10.54	31.89 ± 6.27	51.39 ± 4.78	101.43 ± 39.32	17.01 ± 2.70
Desmodus rotundus	Encapsulated	118.73 ± 38.21	92.52 ± 33.08	28.69 ± 1.89	50.49 ± 40.81	60.95 ± 31.89	60.47 ± 29.22
Gallus gallus	Encapsulated	48.44 ± 22.99	14.31 ± 7.59	10.59 ± 4.02	18.25 ± 7.41	49.07 ± 15.77	57.00 ± 19.62
Lemur catta	Encapsulated	25.86 ± 5.36	17.52 ± 4.57	18.00 ± 12.49	72.21 ± 7.13	93.44 ± 40.89	26.40 ± 5.89
Numida meleagris	Encapsulated	22.44 ± 4.77	12.09 ± 0.90	8.19 ± 2.05	49.99 ± 9.59	46.69 ± 14.19	36.67 ± 7.12
Porphyrio porphyrio	Encapsulated	24.51 ± 2.78	9.87 ± 1.32	8.10 ± 3.07	49.79 ± 38.81	33.40 ± 8.65	30.58 ± 10.92

Propithecus coquereli	Encapsulated	17.06 ± 6.65	86.76 ± 34.01	37.61 ± 12.60	69.02 ± 15.58	128.36 ± 31.95	11.90 ± 4.46
Varecia variegata	Encapsulated	38.18 ± 20.03	22.40 ± 9.05	28.04 ± 10.70	108.72 ± 7.33	87.90 ± 31.34	18.66 ± 5.86
Coturnix japonica	Encapsulated	15.17 ± 4.50	20.72 ± 3.22	21.10 ± 13.27	45.78± 29.68	39.68 ± 15.68	28.55 ± 19.59
Haematopus ostralegus	Encapsulated	37.43 ± 16.23	21.98 ± 3.29	14.72 ± 1.78	28.13 ± 29.64	15.60 ± 7.85	21.82 ± 11.38
Panthera tigris	Encapsulated	23.85 ± 5.97	11.39 ± 5.97	6.54 ± 3.40	85.06 ± 61.61	62.64 ± 19.88	40.99 ± 28.64
Vanellus vanellus	Encapsulated	29.06 ± 15.43	26.19 ± 11.33	9.66 ± 5.74	123.45 ± 28.16	65.75 ± 20.03	44.16 ± 18.23
Colinus virginianus	Encapsulated	38.87 ± 19.95	23.10 ± 8.77	19.61 ± 9.80	63.45 ± 21.63	30.49 ± 16.91	25.94 ± 15.06
Coturnix chinensis	Encapsulated	41.89 ± 9.01	16.12 ± 4.83	12.10 ± 5.11	46.75 ± 16.15	38.42 ± 13.54	38.57 ± 14.10
Didelphis virginiana	Encapsulated	67.77 ± 29.13	50.36 ± 17.46	18.20 ± 10.67	88.88 ± 19.03	49.31 ± 19.61	33.09 ± 9.94
Meleagris gallopavo	Encapsulated	42.35 ± 9.19	13.65 ± 1.81	7.12 ± 3.67	26.44 ± 9.12	30.44 ± 14.15	29.58 ± 9.91
Dromaius novaehollandiae	Encapsulated	21.88 ± 6.02	6.49 ± 0.62	4.81 ± 0.76	43.01 ± 8.25	53.28 ± 32.23	29.68 ± 11.68
Saimiri sciureus	Encapsulated	81.24 ± 18.25	51.49 ± 17.99	22.73 ± 4.62	71.55 ± 17.05	101.40 ± 33.37	39.37 ± 9.06

Table 3. Results from non-phylogenetic Mann–Whitney *U* tests and comparisons of linear mixed-effects models. Mann–Whitney *U* tests were used to compare species-mean CV^* of limb loading variables between tetrapods with encapsulated versus unencapsulated Golgi tendon organ morphology. Linear mixed-effects models were used to assess the relationship between the variables of interest with species and subject as random effects, and Golgi tendon organ morphology (i.e., encapsulated versus unencapsulated), substrate, number of hindlimb substrate reaction forces analyzed, body mass, dimensionless speed, variation in dimensionless speed, and contact time as fixed effects. Model (degrees of freedom = 11) comparison was constrained to a single null (degrees of freedom = 10) that did not include Golgi tendon organ morphology as a fixed effect.

Variable	Mann–Whitney *U* test (*P*-value)	Linear mixed-effects model	Akaike's information criterion	χ^2 value	Comparison of Linear mixed-effects models (*P*-value)
Peak braking force CV^*	< 0.001	Null	138.02	31.86	<0.001
		Model	108.16		
Peak propulsive force CV^*	< 0.001	Null	40.75	26.77	<0.001
		Model	15.98		
Peak medial force CV^*	0.044	Null	69.07	9.43	0.002
		Model	61.63		
Peak lateral force CV^*	0.640	Null	22.06	4.53	0.033
		Model	19.53		
Peak vertical force CV^*	0.004	Null	24.24	6.94	0.008
		Model	19.30		
Timing of peak braking force CV^*	< 0.001	Null	-30.39	16.55	<0.001
		Model	-44.95		
Timing of braking to propulsive transition CV^*	< 0.001	Null	-18.23	25.55	<0.001
		Model	-41.78		
Timing of peak propulsive force CV^*	< 0.001	Null	36.01	30.89	<0.001
		Model	7.12		
Timing of peak medial force CV^*	< 0.001	Null	43.57	5.73	0.017
		Model	39.84		
Timing of peak lateral force CV^*	0.359	Null	-8.30	3.63	0.057
		Model	-9.93		
Timing of peak vertical force CV^*	0.004	Null	7.30	0.02	0.890
		Model	9.28		

Table 4: Evolutionary models fit to residual limb loading and stride cycle CV^*. Residuals are from regressions of $\log_{10}$ limb loading and stride cycle duration CV^* on $\log_{10}$ mass, $\log_{10}$ speed, and $\log_{10}$ speed CV^*. Bolded models have the most support. Values presented are mean ± standard deviation based on running the analysis on 100 trees to account for phylogenetic uncertainty. Variables defined as follows: σ^2 = Brownian motion rate parameter, α = strength of pull towards trait optimum under OU model, $T_{1/2}$ = phylogenetic half-life, θ = trait optima. Models as follows: BM1 = single rate Brownian motion, BM-M = two rate Brownian motion, OU-1 = single optimum Ornstein-Uhlenbeck, OU-M = two optima Ornstein-Uhlenbeck.

Variable	Model	σ^2	α	$T_{1/2}$	θ	Akaike's information criterion	Akaike Weights
Peak braking force CV^*	BM1	1.0e-3±7.3e-5			0.00±0.00	13.6±2.5	0.15±0.06
	BM-M	1.5e-3±1.3e-4, 0.8e-3±5.7e-5			-0.01±0.00	13.5±2.4	0.15±0.07
	OU-1	1.3e-3±1.6e-4	3.1e-3±9.2e-4	224	-0.05±0.01	13.2±1.5	0.15±0.01
	OU-M	**1.5e-3±2.3e-4**	**5.9e-3±1.7e-3**	**117**	**0.10±0.01, -0.88±0.17**	**10.7±1.3**	**0.55±0.12**
Peak propulsive force CV^*	BM1	6.3e-4±2.2e-5			0.00±0.00	-12.6±1.0	0.00±0.00
	BM-M	5.9e-4±4.5e-5, 6.5e-4±1.6e-5			0.00±0.00	-10.4±1.0	0.00±0.00
	OU-1	9.5e-4±2.6e-5	6.7e-3±1.4e-4	103	0.00±0.01	-18.6±0.9	0.02±0.01
	OU-M	**1.6e-3±8.1e-5**	**2.1e-2±1.3e-3**	**33**	**0.14±0.00, -0.23±0.02**	**-27.3±1.0**	**0.98±0.01**
Peak medial force CV^*	BM1	1.8e-3±3.2e-4			0.00±0.00	44.3±7.6	0.00±0.00
	BM-M	8.7e-4±5.8e-4, 2.2e-3±2.2e-4			-0.01±0.00	40.0±10.8	0.00±0.00
	OU-1	**8.3e-3±1.1e-3**	**6.5e-2±2.0e-2**	**11**	**0.13±0.04**	**10.2±11.8**	**0.68±0.01**
	OU-M	9.0e-3±1.3e-3	7.1e-2±1.9e-2	10	0.08±0.01, 0.16±0.07	11.8±12.9	0.32±0.01
Peak lateral force CV^*	BM1	3.0e-3±8.7e-4			0.00±0.00	72.1±12.6	0.00±0.00
	BM-M	2.0e-3±1.5e-3, 3.5e-3±6.2e-4			-0.01±0.00	70.1±14.5	0.00±0.00
	OU-1	1.6e-2±3.2e-3	8.0e-2±3.0e-2	9	0.23±0.01	34.5±19.4	0.02±0.02
	OU-M	**2.6e-2±6.3e-3**	**1.6e-1±6.2e-2**	**4**	**0.02±0.02, 0.34±0.10**	**26.7±18.4**	**0.98±0.03**
	BM1	1.1e-3± 7.7e-5			0.00±0.00	20.0±2.1	0.00±0.00
	BM-M	2.8e-4 ±4.1e-5, 1.5e-3±1.0e-4			0.01±0.00	8.6±2.7	0.00±0.00

Peak vertical force CV^*	**OU-1**	**2.4e-3±1.6e-4**	**1.8-2±1.0e-3**	**39**	**0.02±0.02**	**-1.0±2.7**	**0.53±0.08**
	OU-M	2.5e-3±1.7e-4	2.0e-2±1.7e-3	35	0.10±0.01, -0.04±0.03	-0.7±3.3	0.47±0.09
Timing of peak braking force CV^*	BM1	3.0e-3±9.1e-4			0.00±0.00	71.5±13.4	0.00±0.00
	BM-M	1.7e-3±1.4e-3, 3.6e-3±7.4e-4			0.00±0.00	68.2±16.3	0.00±0.00
	OU-1	**5.5e-2±1.7e-2**	**4.7-1±1.8e-1**	**1.5**	**0.02±0.01**	**8.5±16.3**	**0.52±0.00**
	OU-M	6.0e-2±1.5e-2	5.5e-1±2.0e-1	1.3	0.05±0.01, 0.00±0.11	8.4±17.0	0.48±0.00
Timing of braking to propulsive transition CV^*	BM1	1.3e-3±3.3e-5			0.00±0.00	29.0±1.7	0.00±0.00
	BM-M	2.8e-4±1.8e-5, 1.8e-3±4.7e-5			0.01±0.00	16.2±2.0	0.01±0.01
	OU-1	2.7e-3±2.3e-4	1.7e-2±2.0e-3	41	-0.05±0.01	9.8±1.6	0.13±0.03
	OU-M	**4.4e-3±3.7e-4**	**3.5e-2±3.4e-3**	**20**	**0.07±0.00, -0.16±0.01**	**6.0±1.3**	**0.86±0.04**
Timing of peak propulsive force CV^*	BM1	1.5e-3±1.6e-4			0.00±0.00	33.7±4.3	0.00±0.00
	BM-M	5.7e-4±2.9e-4, 1.9e-3±1.2e-4			0.02±0.00	27.5±7.4	0.00±0.00
	OU-1	2.7e-3±2.2e-4	1.4e-2±1.2e-3	50	-0.08±0.02	16.0±5.7	0.01±0.01
	OU-M	**3.7e-3±3.7e-4**	**2.8e-2±1.4e-3**	**25**	**0.09±0.01, -0.27±0.05**	**7.4±5.7**	**0.99±0.01**
Timing of peak medial force CV^*	BM1	2.2e-3±5.8e-4			0.00±0.00	54.7±11.7	0.00±0.00
	BM-M	1.4e-3±9.2e-4, 2.6e-3±4.6e-4			0.00±0.00	53.6±13.2	0.01±0.00
	OU-1	**1.0e-2±1.6e-3**	**5.7e-2±1.7e-2**	**12**	**0.13±0.06**	**27.0±16.0**	**0.69±0.09**
	OU-M	1.1e-2±2.2e-3	6.2e-2±1.5e-2	11	0.10±0.01, 0.16±0.10	28.7±15.4	0.31±0.09
Timing of peak lateral force CV^*	BM1	9.2e-4±8.5e-5			0.00±0.00	8.2±3.4	0.00±0.00
	BM-M	4.2e-4±1.3e-4, 1.1e-3±7.4e-5			0.00±0.00	4.6±5.0	0.01±0.00
	OU-1	**1.7e-3±1.4e-4**	**1.2e-2±3.7e-4**	**58**	**-0.06±0.02**	**-5.8±4.1**	**0.65±0.07**
	OU-M	1.8e-3±1.1e-4	1.4e-2±1.4e-3	50	-0.11±0.00, 0.01±0.04	-4.5±4.6	0.34±0.07
Timing of peak vertical force CV^*	BM1	1.7e-3±9.4e-5			0.00±0.00	41.0±1.6	0.00±0.00
	BM-M	6.4e-4±6.6e-5, 2.1e-3±1.2e-4			-0.01±0.00	36.0±1.9	0.00±0.00
	OU-1	**4.1e-3±1.7e-4**	**2.3e-2±1.9e-3**	**30**	**0.07±0.02**	**20.0±3.0**	**0.76±0.01**
	OU-M	4.1e-3±1.7e-4	2.3e-2±1.8e-3	30	0.07±0.01, 0.08±0.03	22.0±2.9	0.24±0.01
	BM1	3.9e-3±1.4e-3			0.00±0.00	85.8±15.6	0.00±0.00
	BM-M	3.3e-3±2.5e-3, 4.3e-3±9.0e-4			0.01±0.01	86.3±16.5	0.00±0.00

Stride cycle duration CV^*	OU-1	2.2e-1±3.6e-1	1.6e0±2.6e0	0.43	-0.24±0.01	37.1±27.4	0.00±0.00
	OU-M	**1.4e0±1.3e0**	**1.0e1±6.6e0**	**0.06**	**0.05±0.02, -0.38±0.14**	**17.1±28.7**	**1.00±0.00**

Table 5: Phylogenetic generalized least squares (PGLS) models of the relationships between coefficient of variation (CV^*) of stride cycle duration (y) and CV^* all limb loading variables (x). Bolded models have the most support. Values presented are means based on running the analysis on 100 trees to account for phylogenetic uncertainty (standard deviations not shown, but were at least an order of magnitude smaller than the mean for all parameters). Variables defined as follows: σ^2 = Brownian motion rate parameter, α = strength of pull towards trait optimum under OU model, λ = Pagel's lambda. Models as follows: λ= Pagel's lambda model, OU = single optimum Ornstein-Uhlenbeck.

Variable	Model	σ^2	α	λ	Akaike's information criterion	Akaike Weights	Intercept	Slope	*t*-value	*P*-value
Peak braking force CV^*	**λ**	**0.00013**		**0.34**	**-12.7**	**1.00**	**1.243**	**0.018**	**0.21**	**0.835**
	OU	0.10381	1.000		-1.1	0.00	1.151	0.053	0.05	0.497
Peak propulsive force CV^*	**λ**	**0.00012**		**0.28**	**-13.9**	**0.98**	**1.057**	**0.136**	**1.15**	**0.255**
	OU	0.09238	1.000		-5.3	0.02	0.806	0.288	2.66	0.010
Peak medial force CV^*	**λ**	**0.00012**		**0.32**	**-15.0**	**1.00**	**1.634**	**-0.203**	**-1.51**	**0.137**
	OU	0.09840	1.00		-1.8	0.00	1.719	0.274	-1.82	0.077
Peak lateral force CV^*	**λ**	**0.00013**		**0.36**	**-13.8**	**1.00**	**1.502**	**-0.138**	**-1.04**	**0.305**
	OU	0.09970	1.00		-1.1	0.00	1.626	-0.237	-1.59	0.126
Peak vertical force CV^*	**λ**	**0.00013**		**0.31**	**-15.1**	**0.98**	**1.042**	**0.196**	1.56	**0.126**
	OU	0.08996	1.00		-6.8	0.02	0.846	0.347	2.96	0.006
Timing of peak braking force CV^*	**λ**	**0.00013**		**0.31**	**-13.5**	**1.00**	**1.113**	**0.094**	**0.93**	**0.355**
	OU	0.10005	1.00		-0.9	0.00	0.995	0.153	1.55	0.127
Timing of braking to propulsive transition CV^*	**λ**	**0.00013**		**0.32**	**-13.5**	**1.00**	**1.153**	**0.078**	**0.893**	**0.376**
	OU	0.10267	1.00		0.5	0.00	1.116	0.088	1.032	0.308
Timing of peak	**λ**	**0.00013**		**0.32**	**-13.3**	**1.00**	**1.178**	**0.074**	**0.76**	**0.448**
	OU	0.10080	1.00		-0.5	0.00	1.077	0.136	1.43	0.158

propulsive force CV^*										
Timing of peak medial force CV^*	**λ**	**0.00014**		**0.35**	**-12.8**	**1.00**	**1.358**	**-0.042**	**-0.36**	**0.722**
	OU	0.10416	1.00		1.3	0.00	1.347	-0.057	-0.44	0.672
Timing of peak lateral force CV^*	**λ**	**0.00013**		**0.32**	**-12.8**	**0.98**	**1.357**	**-0.046**	**-0.37**	**0.713**
	OU	0.09427	1.00		-4.2	0.02	1.738	-0.289	-2.43	0.020
Timing of peak vertical force CV^*	**λ**	**0.00013**		**0.34**	**-13.4**	**1.00**	**1.151**	**0.083**	**0.803**	**0.426**
	OU	0.09998	1.00		-0.9	0.00	0.983	0.180	1.586	0.124

Table S1. Statistical parameters derived from linear mixed-effects models demonstrating the statistical importance of various fixed effects. Values in bold illustrate fixed effects that significantly influence each respective response variable.

Response variable	Fixed effect	Estimate	Standard Error	*t* value	*F* value	*P* value
Peak braking force CV^*	(Intercept)	1.28	0.17	-	-	-
	Golgi tendon organ morphology	0.58	0.09	6.56	37.19	**< 0.001**
	Substrate	0.27	0.08	3.43	10.24	**0.002**
	Dimensionless speed	-0.04	0.14	-0.27	0.02	0.892
	Count	0.00	0.00	1.26	1.71	0.195
	Dimensionless speed CV^*	0.12	0.07	1.71	2.41	0.123
	Mass	-0.08	0.05	-1.55	2.16	0.148
	Contact time	0.13	0.19	0.69	0.49	0.485
Peak propulsive force CV^*	(Intercept)	1.11	0.14	-	-	-
	Golgi tendon organ morphology	0.44	0.08	5.45	29.72	**< 0.001**
	Substrate	0.10	0.07	1.37	1.87	0.178
	Dimensionless speed	0.00	0.13	0.03	0.00	0.979
	Count	0.00	0.00	1.72	2.97	0.088
	Dimensionless speed CV^*	0.15	0.05	2.78	7.72	**0.006**
	Mass	-0.05	0.04	-1.03	1.07	0.306
	Contact time	-0.02	0.17	-0.11	0.01	0.910
Peak medial force CV^*	(Intercept)	1.53	0.16	-	-	-
	Golgi tendon organ morphology	0.24	0.08	2.96	8.74	**0.005**
	Substrate	-0.07	0.07	-0.95	0.90	0.349
	Dimensionless speed	0.07	0.13	0.53	0.28	0.597
	Count	0.01	0.00	3.08	9.50	**0.003**
	Dimensionless speed CV^*	0.07	0.06	1.18	1.38	0.241
	Mass	0.06	0.05	1.23	1.50	0.227
	Contact time	0.16	0.18	0.91	0.82	0.370
Peak lateral force CV^*	(Intercept)	1.59	0.14	-	-	-
	Golgi tendon organ morphology	0.16	0.08	2.04	4.17	**0.047**

	Substrate	0.32	0.07	4.74	22.49	**< 0.001**
	Dimensionless speed	0.25	0.12	2.05	4.20	**0.046**
	Count	0.01	0.00	2.94	8.66	**0.004**
	Dimensionless speed CV^*	0.03	0.06	0.59	0.35	0.555
	Mass	-0.09	0.05	-1.90	3.60	0.063
	Contact time	0.38	0.16	2.35	5.52	**0.022**
Peak vertical force CV^*	(Intercept)	0.72	0.15	-	-	-
	Golgi tendon organ morphology	0.24	0.09	2.56	6.57	**0.014**
	Substrate	-0.12	0.08	-1.48	2.18	0.147
	Dimensionless speed	0.11	0.14	0.75	0.56	0.458
	Count	0.00	0.00	1.59	2.54	0.114
	Dimensionless speed CV^*	0.26	0.05	4.77	22.72	**< 0.001**
	Mass	-0.04	0.05	-0.83	0.68	0.413
	Contact time	-0.10	0.19	-0.51	0.26	0.609
Timing of peak braking force CV^*	(Intercept)	1.43	0.12	-		
	Golgi tendon organ morphology	0.33	0.08	4.39	19.27	**< 0.001**
	Substrate	0.17	0.07	2.49	6.22	**0.016**
	Dimensionless speed	-0.06	0.11	-0.57	0.32	0.573
	Count	0.00	0.00	0.69	0.48	0.491
	Dimensionless speed CV^*	0.09	0.04	2.17	4.70	**0.032**
	Mass	-0.14	0.04	-3.17	10.08	**0.002**
	Contact time	0.24	0.15	1.59	2.52	0.116
Timing of braking to propulsive transition CV^*	(Intercept)	1.12	0.12	-	-	-
	Golgi tendon organ morphology	0.39	0.07	5.49	27.62	**< 0.001**
	Substrate	0.40	0.06	6.25	34.45	**< 0.001**
	Dimensionless speed	-0.19	0.11	-1.73	2.67	0.11
	Count	0.00	0.00	0.48	0.29	0.59
	Dimensionless speed CV^*	0.05	0.04	1.26	1.77	0.19
	Mass	-0.17	0.04	-4.03	13.81	**< 0.001**
	Contact time	0.09	0.15	-.61	0.28	0.60
Timing of peak	(Intercept)	0.78	0.13	-	-	-
	Golgi tendon organ morphology	0.40	0.07	5.84	34.09	**< 0.001**

propulsive force CV^*	Substrate	0.35	0.06	5.84	34.05	**< 0.001**
	Dimensionless speed	-0.19	0.11	-1.78	3.16	0.083
	Count	0.00	0.00	-0.27	0.07	0.788
	Dimensionless speed CV^*	0.14	0.05	2.69	7.25	**0.008**
	Mass	-0.12	0.04	-2.94	8.66	**0.005**
	Contact time	0.05	0.15	0.36	0.13	0.722
Timing of peak medial force CV^*	(Intercept)	1.80	0.16	-	-	-
	Golgi tendon organ morphology	0.22	0.10	2.31	5.32	**0.025**
	Substrate	0.03	0.09	0.33	0.11	0.743
	Dimensionless speed	-0.06	0.15	-0.43	0.19	0.668
	Count	0.00	0.00	0.98	0.96	0.329
	Dimensionless speed CV^*	-0.11	0.06	-1.88	3.53	0.062
	Mass	0.02	0.06	0.30	0.09	0.762
	Contact time	0.01	0.20	0.04	0.00	0.967
Timing of peak lateral force CV^*	(Intercept)	1.97	0.12	-	-	-
	Golgi tendon organ morphology	-0.10	0.06	-1.75	3.06	0.087
	Substrate	0.33	0.05	6.24	38.95	**< 0.001**
	Dimensionless speed	0.07	0.09	0.79	0.63	0.433
	Count	0.00	0.00	2.53	6.38	**0.015**
	Dimensionless speed CV^*	-0.13	0.05	-2.72	7.42	**0.007**
	Mass	-0.07	0.04	-1.85	3.42	0.071
	Contact time	0.48	0.13	3.77	14.20	**< 0.001**
Timing of peak vertical force CV^*	(Intercept)	1.59	0.15	-	-	-
	Golgi tendon organ morphology	0.01	0.09	0.13	0.02	0.896
	Substrate	-0.09	0.08	-1.11	1.23	0.273
	Dimensionless speed	0.06	0.14	0.41	0.17	0.682
	Count	0.00	0.00	1.09	1.18	0.280
	Dimensionless speed CV^*	-0.03	0.05	-0.60	0.36	0.547
	Mass	-0.13	0.05	-2.56	6.53	**0.013**
	Contact time	0.24	0.18	1.36	1.84	0.179

-Information not pertinent.

Table S2: Evolutionary models fit to log_{10} limb loading and stride cycle CV* with intraspecific sampling included in the model. Bolded models have the most support. Values presented are mean ± standard deviation based on running the analysis on 100 trees to account for phylogenetic uncertainty. Variables defined as follows: σ^2 = Brownian motion rate parameter, α = strength of pull towards trait optimum under OU model, $T_{1/2}$ = phylogenetic half-life, θ = trait optima. Models as follows: BM1 = single rate Brownian motion, BM-M = two rate Brownian motion, OU-1 = single optimum Ornstein-Uhlenbeck, OU-M = two optima Ornstein-Uhlenbeck.

Variable	Model	σ	α	$T_{1/2}$	θ	Akaike's information criterion	Akaike Weights
Peak braking force CV*	BM1	1.7e-04±6.4e-07			1.5±0.00	78.1±0.02	0.21±0.00
	BM-M	**1.5e-11±3.1e-11 5.0e-04±2.9e-06**			**1.7±0.00**	**77.1±0.04**	**0.34±0.00**
	OU-1	6.0e-04±2.6e-06	0.0077±0.00003	90	1.5±0.00	79.0±0.03	0.13±0.00
	OU-M	3.9e-04±2.1e-06	0.0110±0.00005	63	1.7±0.00 1.2±0.00	77.2±0.01	0.32±0.00
Peak propulsive force CV*	**BM1**	**9.5e-19±9.4e-18**			**1.5±0.00**	**48.3±0.00**	**0.56±0.00**
	BM-M	1.7e-16±6.6e-16 1.9e-15±1.1e-14			1.5±0.00	50.5±0.00	0.18±0.00
	OU-1	5.3e-21±5.7e-21	0.0084±0.00002	83	1.5±0.00	50.5±0.00	0.18±0.00
	OU-M	3.4e-13±9.4e-13	1.2e-8±1.6e-8	5.8e7	1.5±0.00, 1.4e5±2.0e5	52.4±0.00	0.07±0.00
Peak medial force CV*	**BM1**	**2.5e-19±1.7e-18**			**1.7±0.00**	**64.1±0.00**	**0.57±0.00**
	BM-M	2.3e-15±6.9e-15 4.8e-15±1.0e-14			1.7±0.00	66.3±0.00	0.19±0.00
	OU-1	7.9e-22 ±1.6e-22	0.0073±6.0e-6	95	1.7±0.00	66.3±0.00	0.19±0.00
	OU-M	3.4e-12±7.6e-12	1.2e-8±1.8e-8	5.8e7	1.7±0.00 -3.1e5±3.8e+05	68.5±0.00	0.06±0.00
	BM1	**3.7e-17 ± 3.6e-16**			**1.6±0.00**	**55.0±0.00**	**0.57±0.00**

Peak lateral force CV*	BM-M	6.2e-16 ±2.3e-15 7.3e-16 ±1.8e-15			1.6±0.00	57.3±0.00	0.19±0.00
	OU-1	4.1e-20 ±2.9e-20	0.0074±3.8e-6	94	1.6±0.00	57.3±0.00	0.19±0.00
	OU-M	3.8e-13±2.1e-12	9.5e-9±8.7e-9	7.2e7	1.7±0.00, -1.9e5±2.2e5	59.5±0.00	0.06±0.00
Peak vertical force CV*	BM1	5.6e-05±4.3e-07			1.1±0.00	29.5±0.03	0.23±0.00
	BM-M	**5.2e-12±9.5e-12 3.0e-04±3.6e-06**			**1.0±0.00**	**28.0±0.06**	**0.50±0.01**
	OU-1	5.6e-05±3.2e-07	2.2e-6±3.8e-6	3.2e5	1.1±0.00	31.7±0.03	0.08±0.00
	OU-M	1.5e-10±2.3e-10	1.4e-8±2.5e-8	5.0e7	0.7±0.00, 1.7e6±1.9e6	29.9±0.00	0.19±0.00
Timing of peak braking force CV*	BM1	3.8e-05±2.1e-07			1.5±0.00	65.5±0.01	0.33±0.00
	BM-M	3.6e-13±1.7e-12 1.4e-04±4.9e-06			1.6±0.00	67.5±0.05	0.12±0.00
	OU-1	2.6e-04±8.4e-06	0.0099±0.150	70	1.5±0.00	67.1±0.02	0.15±0.00
	OU-M	**2.1e-10±1.5e-09**	**0.0003±0.012**	**2.3e3**	**1.7±0.00, 1.4±0.00**	**65.1±0.00**	**0.40±0.00**
Timing of braking to propulsive transition CV*	BM1	7.3e-05 ±7.7e-07			1.3±0.00	64.1±0.03	0.19±0.00
	BM-M	6.1e-05±5.0e-05 1.2e-04±1.2e-04			1.3±0.03	66.0±0.33	0.07±0.01
	OU-1	8.1e-02 ±1.8e-01	1.2±2.7	0.6	1.2±0.00	63.3±0.03	0.28±0.00
	OU-M	**6.2e-02±1.3e-01**	**1.1±2.4**	**0.6**	**1.4±0.00, 1.2±0.00**	**62.3±0.01**	**0.45±0.01**
Timing of peak propulsive force CV*	BM1	0.00057±1.6e-05			1.2±0.00	71.1±0.59	0.00±0.00
	BM-M	0.00009±3.1e-06 0.00097±3.6e-05			1.2±0.00	68.7±0.55	0.01±0.00
	OU-1	0.17000±3.1e-01	1.4±2.6	0.5	1.1±0.00	60.0±0.19	0.48±0.01
	OU-M	**0.33000±8.3e-01**	**3.0±7.4**	**0.2**	**1.3±0.00, 1.1±0.00**	**59.9±0.15**	**0.51±0.01**
Timing of peak medial force CV*	**BM1**	**1.5e-19±1.4e-18**			**1.7±0.00**	**76.3±0.00**	**0.54±0.02**
	BM-M	1.4e-11± 3.4e-11 1.1e-05± 1.0e-05			1.7±0.00	78.5±0.01	0.18±0.02
	OU-1	4.9e-18 ±8.1e-18	0.008±0.00001	87	1.7±0.00	78.5±0.00	0.18±0.00
	OU-M	3.2e-10±1.8e-09	0.120±0.018	6	1.8±0.00, 1.7±0.00	79.6±0.00	0.11±0.00

Timing of peak lateral force CV*	BM1	4.6e-05±8.1e-06			1.5±0.03	73.6±0.37	0.29±0.03
	BM-M	2.5e-11±5.3e-11 1.2e-04±6.7e-07			1.5±0.00	74.8±0.01	0.16±0.01
	OU-1	7.1e-04±4.8e-05	0.030±0.002	23	1.5±0.00	74.8±0.01	0.16±0.01
	OU-M	**6.3e-04±6.4e-06**	**0.002±0.001**	**347**	**1.9±0.00, 1.5±0.00**	**73.0±0.00**	**0.39±0.02**
Timing of peak vertical force CV*	**BM1**	**3.1e-05±3.1e-07**			**1.3±0.00**	**52.3±0.02**	**0.52±0.00**
	BM-M	7.8e-12 ±1.8e-11 1.3e-04 ±2.1e-06			1.3±0.00	53.7±0.07	0.25±0.00
	OU-1	5.6e-05±4.1e-06	0.0021±0.0003	330	1.3±0.00	54.5±0.03	0.17±0.00
	OU-M	5.6e-05±4.1e-06	0.0020±0.0003	347	1.3±0.00, 1.3±0.01	56.8±0.03	0.05±0.00
Stride cycle duration CV*	BM1	1.7e-04±1.3e-06			1.1±0.00	29.8±0.14	0.15±0.01
	BM-M	8.3e-05±8.0e-07 3.4e-04±4.0e-06			1.1±0.00	29.3±0.14	0.20±0.01
	OU-1	**9.0e-04±6.8e-05**	**0.015±0.001**	**46**	**1.2±0.00**	**28.3±0.13**	**0.34±0.01**
	OU-M	1.2e-03±1.3e-03	0.024±0.028	29	1.1±0.00, 1.2±0.00	28.5±0.14	0.30±0.01

Table S3: Type I error and, statistical power computed from simulations based on the OU-M models fit to each variable. Selection opportunity (η), the discriminably ratio (ϕ) and the signal to noise ratio (SNR) were computed using equations from Cressler et al. (2015).

		Type I error	Power	η	ϕ	SNR
Raw with standard error included	Peak Brake	0.15	1.00	3.9E+00	1.9E+02	3.7E+02
	Peak Accel	0.17	1.00	4.2E-06	6.4E+13	1.3E+11
	Peak Vertical	0.05	1.00	3.3E-06	6.9E+13	1.3E+11
	Peak Lateral	0.1	1.00	4.2E-06	1.4E+13	2.9E+10
	Peak Medial	0.12	1.00	4.9E-06	1.9E+12	4.2E+09
	Time Brake	0.26	1.00	3.9E+02	4.8E+00	9.4E+01
	Time Accel	0.15	1.00	1.1E-01	3.5E+07	1.1E+07
	Time Vertical	0.22	1.00	7.0E-01	4.0E+01	3.4E+01
	Time Lateral	0.17	1.00	4.2E+01	1.5E+08	9.9E+08
	Time Medial	0.22	1.00	7.0E-01	0.0E+00	0.0E+00
	Time BP	0.13	1.00	1.1E+03	1.5E+00	4.8E+01
	Cycle	0.24	1.00	8.4E+00	1.8E+01	5.3E+01
Residual without standard error	Peak Brake	0.16	0.99	2.1E+00	7.1E+01	1.0E+02
	Peak Accel	0.25	1.00	7.4E+00	4.7E+01	1.3E+02
	Peak Vertical	0.17	1.00	5.6E+01	7.0E+00	5.2E+01
	Peak Lateral	0.15	1.00	2.5E+01	3.3E+00	1.7E+01
	Peak Medial	0.17	1.00	7.0E+00	1.1E+01	3.0E+01
	Time Brake	0.19	1.00	9.9E+00	2.3E+01	7.2E+01
	Time Accel	0.06	1.00	1.9E+02	8.7E-01	1.2E+01
	Time Vertical	0.23	1.00	4.9E+00	1.1E+01	2.5E+01
	Time Lateral	0.22	1.00	2.2E+01	1.9E+00	9.0E+00
	Time Medial	0.18	1.00	8.1E+00	5.2E-01	1.5E+00
	Time BP	0.21	1.00	1.2E+01	1.4E+01	4.9E+01
	Cycle	0.15	1.00	3.5E+03	1.4E+00	3.9E+00

Supplementary Figures:

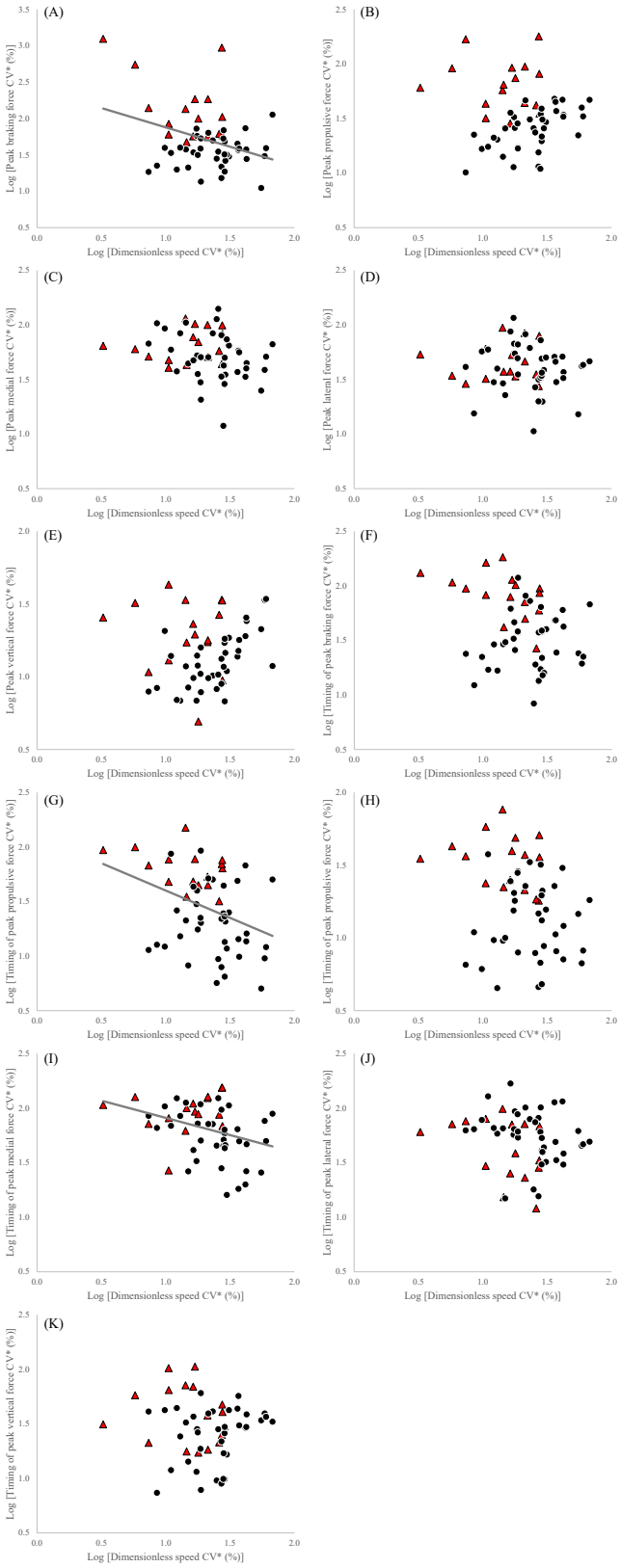

Supplemental Fig. 1. Scatterplots of the species-mean log-transformed coefficient of variation (CV^*) of (A) braking peak force, (B) propulsive peak force, (C) medial peak force, (D) lateral peak force, (E) vertical peak force, (F) timing of braking peak force, (G) timing of the braking to propulsive transition, (H) timing of propulsive peak force, (I) timing of medial peak force, (J) timing of lateral peak force, and (K) timing of vertical peak force as a function of species-mean log-transformed dimensionless speed CV^* (%). There is a significant negative relationship between species-mean log-transformed dimensionless speed CV^* (m/s) and peak braking force CV^* (y = -0.53x + 2.41; P = 0.008), the braking to propulsive transition CV^* (y = -0.50x + 2.10; P = 0.007) and the timing of peak medial force CV^* (y = -0.31x + 2.22; P = 0.011). Species with encapsulated Golgi tendon organs (GTO) are illustrated as black circles and species with unencapsulated GTOs are red triangles.

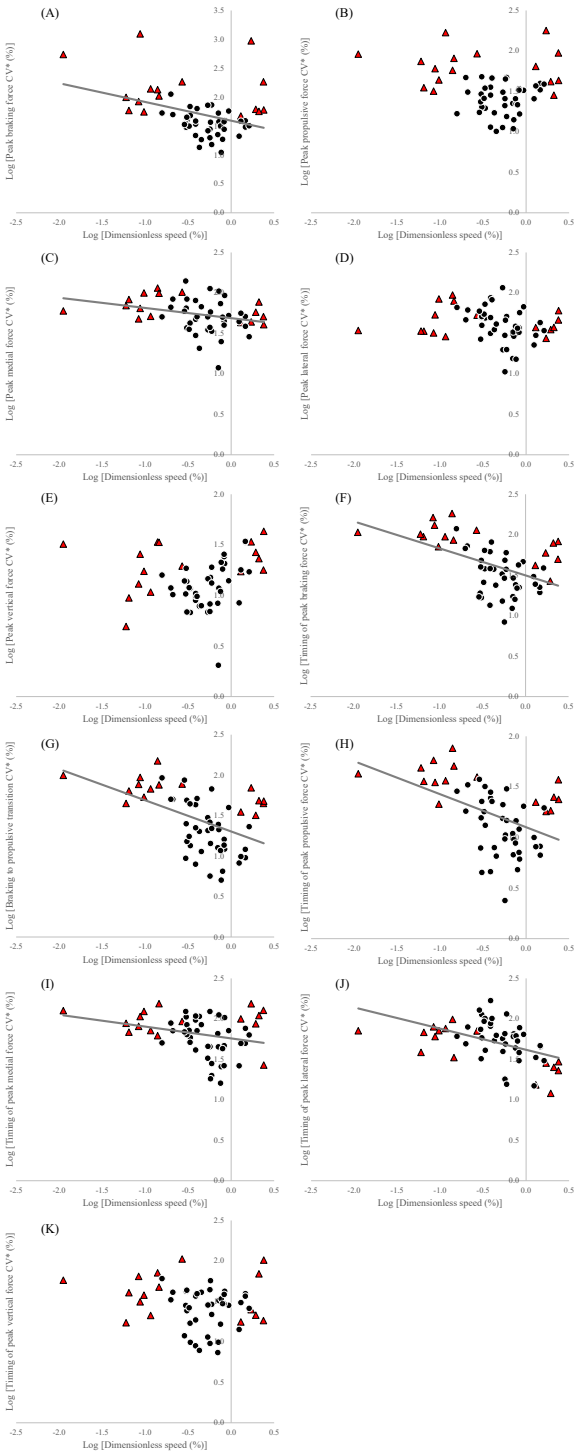

Supplemental Fig. 2. Scatterplots of the species-mean log-transformed coefficient of variation (CV^*) of (A) braking peak force, (B) propulsive peak force, (C) medial peak force, (D) lateral peak force, (E) vertical peak force, (F) timing of braking peak force, (G) timing of the braking to propulsive transition, (H) timing of propulsive peak force, (I) timing of medial peak force, (J) timing of lateral peak force, and (K) timing of vertical peak force as a function of species-mean log-transformed dimensionless speed. There is a significant negative relationship between species-mean log-transformed dimensionless speed (m/s) and peak braking force CV^* (y = -0.32x + 1.59; P = 0.005), peak medial force CV^* (y = -0.13x + 1.69; P = 0.035), the timing of peak braking force CV^* (y = -0.33x + 1.50; $P < 0.001$), the braking to , propulsive transition CV^* (y = -0.39x + 1.30; $P < 0.001$), the timing of peak propulsive force CV^* (y = -0.33x + 1.10; $P < 0.001$), the timing of peak medial force CV^* (y = -0.15x + 1.76; P = 0.041), and the timing of peak lateral force CV^* (y = -0.26x + 1.62; $P < 0.001$). Species with encapsulated Golgi tendon organs (GTO) are illustrated as black circles and species with unencapsulated GTOs are red triangles.

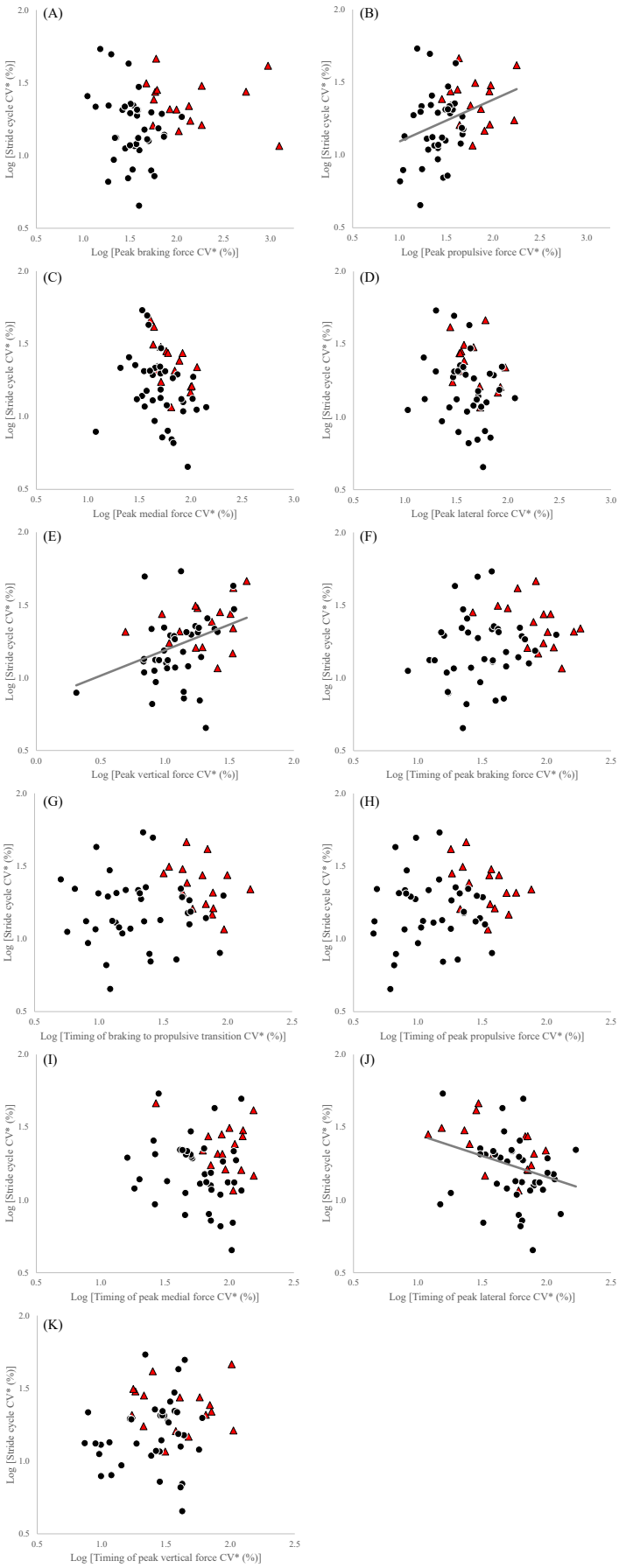

Supplemental Fig. 3. Scatterplots of the log-transformed species-mean coefficient of variation (CV^*) of stride cycle duration as a function of log-transformed CV^* of (A) braking peak force, (B) propulsive peak force, (C) medial peak force, (D) lateral peak force, (E) vertical peak force, (F) timing of braking peak force, (G) timing of the braking to propulsive transition, (H) timing of propulsive peak force, (I) timing of medial peak force, (J) timing of lateral peak force, and (K) timing of vertical peak force. There is a significant relationship between CV^* of stride cycle duration and peak propulsive force CV^* (y = 0.29x + 0.81; P = 0.009), peak vertical force CV^* (y = 0.35x + 0.84; P = 0.005) and the timing of peak lateral force CV^* (y = -0.29x + 1.74; P = 0.016). The solid line in each graph represents the best fit line. Species with encapsulated Golgi tendon organs (GTO) are illustrated as black circles and species with unencapsulated GTOs are red triangles.